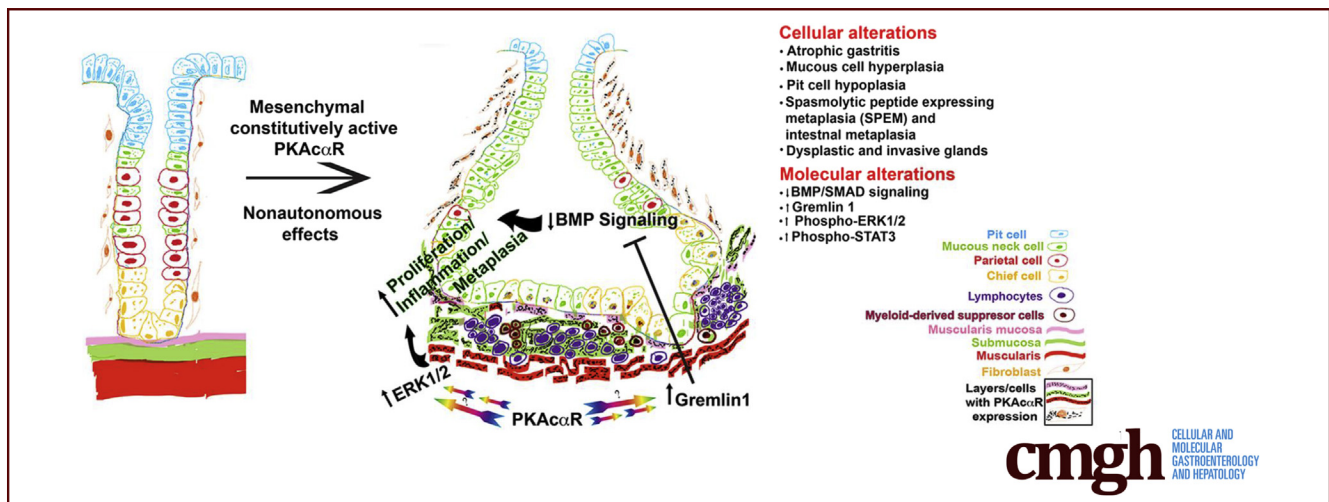


## ORIGINAL RESEARCH

## Elevated Protein Kinase A Activity in Stomach Mesenchyme Disrupts Mesenchymal-epithelial Crosstalk and Induces Preneoplasia

Pawan Puri,<sup>1</sup> Garfield Grimmer,<sup>1</sup> Rawah Faraj,<sup>1</sup> Laurielle Gibson,<sup>1</sup> Ebony Gilbreath,<sup>2</sup> and Bradley K. Yoder<sup>3</sup><sup>1</sup>Department of Biomedical Sciences, Tuskegee University College of Veterinary Medicine, Tuskegee, Alabama; <sup>2</sup>Department of Pathobiology, College of Veterinary Medicine, Tuskegee University, Tuskegee, Alabama; and <sup>3</sup>Department of Cell, Developmental, and Integrative Biology, Heersink School of Medicine, University of Alabama, Birmingham, Alabama

## SUMMARY

Our studies demonstrate for the first time that Protein Kinase A (PKA) executes gastric mesenchymal-epithelial crosstalk. Mice expressing a constitutively active PKA mutant in the gastric mesenchyme develop classic preneoplastic lesions and marked chronic inflammation, factors strongly associated with gastric cancer.

**BACKGROUND & AIMS:** Mesenchymal-epithelial crosstalk (MEC) in the stomach is executed by pathways such as bone morphogenetic protein (BMP) and extracellular signal-regulated kinase (ERK). Mis-regulation of MEC disrupts gastric homeostasis and causes tumorigenesis. Protein Kinase A (PKA) crosstalks with BMP and ERK signaling; however, PKA function(s) in stomach development and homeostasis remains undefined.

**METHODS:** We generated a novel Six2-Cre<sup>+/+</sup>-PKAαR<sup>fl/wt</sup> (CA-PKA) mouse in which expression of constitutive-active PKAαR was induced in gastric mesenchyme progenitors. Lineage tracing determined spatiotemporal activity of Six2-Cre in the stomach. For phenotyping CA-PKA mice histological,

co-immunofluorescence, immunoblotting, mRNA sequencing, and bioinformatics analyses were performed.

**RESULTS:** Lineage tracing showed that Six2-Cre activity in the stomach is restricted to the mesenchymal compartment. CA-PKA mice showed disruption of gastric homeostasis characterized by aberrant mucosal development and epithelial hyperproliferation; ultimately developing multiple features of gastric corpus preneoplasia including decreased parietal cells, mucous cell hyperplasia, spasmolytic peptide expressing metaplasia with intestinal characteristics, and dysplastic and invasive cystic glands. Furthermore, mutant corpus showed marked chronic inflammation characterized by infiltration of lymphocytes and myeloid-derived suppressor cells along with the upregulation of innate and adaptive immune system components. Striking upregulation of inflammatory mediators and STAT3 activation was observed. Mechanistically, we determined there is an activation of ERK1/2 and downregulation of BMP/SMAD signaling characterized by marked upregulation of BMP inhibitor gremlin 1.

**CONCLUSIONS:** We report a novel role of PKA signaling in gastric MEC execution and show that PKA activation in the gastric mesenchyme drives preneoplasia by creating a proinflammatory and proliferative microenvironment associated

with the downregulation of BMP/SMAD signaling and activation of ERK1/2. (*Cell Mol Gastroenterol Hepatol* 2022;14:643–668; <https://doi.org/10.1016/j.jcmgh.2022.06.001>)

**Keywords:** Gastric Metaplasia; Gastric Preneoplasia; PKA.

See editorial on page 722.

**M**esenchymal-epithelial interactions (MECs) play crucial roles in stomach function in the healthy and diseased states.<sup>1,2</sup> Mouse stomach mucosa consists of three regions lined by epithelia with distinct features. The non-glandular forestomach is lined by stratified squamous epithelium, whereas the glandular portions, corpus, and antrum are lined by columnar epithelium. Corpus glands consist of mucus-secreting foveolar/pit cells and mucous neck cells, acid-secreting parietal cells, enzyme precursor-secreting chief cells, and endocrine cells such as enterocromaffin-like (ECL) and delta (D) cells.<sup>3</sup> Antral glands consist of mucus-secreting cells and gastrin-secreting G cells. The mesenchymal population, present in proximity to the epithelium, consists of various stromal cell types, including fibroblasts and myofibroblasts that secrete key paracrine factors.<sup>1</sup> Numerous signaling pathways such as bone morphogenetic protein (BMP), fibroblast growth factor, and sonic hedgehog contribute to the MEC.<sup>3</sup> Misregulation of the MEC can disrupt development and homeostasis and can lead to tumorigenesis.<sup>1,3</sup> BMP signaling initiated from both mesenchymal and epithelial compartments is crucial for gastric development and function.<sup>2</sup> Mesenchymal-specific loss of BMP signaling causes disruption of the gland architecture and function, leading to the development of spasmolytic polypeptide expressing metaplasia (SPEM) and intestinal metaplasia, precursor lesions associated with gastric adenocarcinoma.<sup>4</sup> Inhibition of BMP signaling in parietal cells by transgenic expression of a BMP inhibitor noggin results in inflammation, hyperproliferation, and decreased parietal cell number ultimately leading to SPEM.<sup>5,6</sup> Transgenic mice expressing noggin also show increased inflammatory response following *Helicobacter Pylori* (*H. Pylori*) infection indicating an anti-inflammatory role of BMP signaling in the stomach.<sup>7</sup>


*H. Pylori*-induced inflammation is the major predisposing factor for gastric adenocarcinoma.<sup>8–10</sup> More recently, it has been shown that *H. Pylori* causes inflammation by altering the amounts of a BMP ligand, BMP2, and multiple BMP antagonists that are all important components of the niche surrounding gastric stem cells.<sup>11</sup> A precisely balanced level of the BMP ligands and antagonists are released by distinct stromal cell population localized in close proximity to the gland surface and base, respectively.<sup>11</sup> *H. Pylori* is known to invade deep into the gastric glands and disrupts the BMP signaling components of the niche by altering the number and location of stromal cells.<sup>11,12</sup> Although the role of misregulation of BMP signaling is well-established in *H pylori*-induced gastric pathology, the mechanisms that regulate BMP signaling and/or the stromal population that secrete

BMP components remain undefined. In addition to BMP signaling, mis-regulation of extracellular signal-regulated kinase (ERK) signaling in gastric stromal fibroblasts is also known to disrupt the niche created by stromal cells and contribute to the pathogenesis of gastric cancer.<sup>13</sup> Protein kinase A (PKA) signaling is known to crosstalk with both BMP and ERK signaling.<sup>14–17</sup> Therefore, we hypothesized that mesenchymal PKA signaling plays a key regulatory role in the functioning of gastric stromal cell populations and their crosstalk with the epithelium. Furthermore, aberrant increases in PKA activity are sufficient to cause tumors in mesenchyme (bone), endocrine (adrenal), or epithelial (breast) tissues.<sup>18–20</sup> However, PKA contributions to gastric preneoplastic lesions and/or cancer remain unknown. In the stomach, PKA is critical for histamine-stimulated gastric acid production in parietal cells.<sup>21</sup> However, PKA-specific functions in other gastric cells/compartments have not been well-defined.

PKA, one of the main effectors of the second messenger cAMP, exists as an inactive complex of 2 catalytic and 2 regulatory subunits.<sup>22</sup> Ligand-stimulated cAMP production and cAMP binding to PKA regulatory subunits releases and activates catalytic subunits. Mice have 3 genes with multiple splice variants encoding PKA catalytic subunits. Of the various isoforms, PKA $\alpha$ 1 is ubiquitously expressed and predominantly accounts for most of the PKA activity in almost all tissues.<sup>22</sup>

To evaluate PKA signaling in gastric cells/compartments, we generated a novel mutant mouse model in which a constitutively active PKA mutant PKA $\alpha$ R is activated by a Six2-promoter-driven Cre recombinase.<sup>23,24</sup> In the PKA catalytic subunit mutant, PKA $\alpha$ R, a mis-sense mutation, hampers its ability to bind with regulatory subunit, leading to constitutive activation.<sup>23</sup> Expression of a single copy of PKA $\alpha$ R, specifically in hepatocytes, osteoblasts, and mammary glands, revealed PKA functions in glucose metabolism, bone anabolism, mammary gland development, and tumorigenesis, respectively.<sup>23,25–27</sup> Our results show that Six2-Cre induced constitutively active PKA $\alpha$ R in the stomach mesenchyme nonautonomously disrupts gastric homeostasis, characterized by increased epithelial proliferation and aberrant epithelial maldevelopment, ultimately leading to gastric preneoplasia.

**Abbreviations used in this paper:** AB, Alcian blue; ACTA1, alpha smooth muscle actin; BMP, bone morphogenetic protein; CA-PKA, Six2Cre<sup>+/+</sup>-PKA $\alpha$ R<sup>fl/wt</sup>; CHGA, chromogranin A; D, delta; ECL, enterocromaffin-like; ERK, extracellular signal-regulated kinase; GIF, gastric intrinsic factor; GO, Gene Ontology; IF, immunofluorescence; MEC, mesenchymal-epithelial crosstalk; MRNA seq, mRNA sequencing; PAS, periodic acid-Schiff; PDGFRA, platelet-derived growth factor receptor alpha; PIGR, polymeric immunoglobulin receptor; PJS, Peutz-Jeghers Syndrome; PKA, Protein Kinase A; RFP, red fluorescent protein; SPEM, spasmolytic peptide expressing metaplasia; VIM, vimentin.

 Most current article

© 2022 The Authors. Published by Elsevier Inc. on behalf of the AGA Institute. This is an open access article under the CC BY-NC-ND license (<http://creativecommons.org/licenses/by-nc-nd/4.0/>).

2352-345X

<https://doi.org/10.1016/j.jcmgh.2022.06.001>

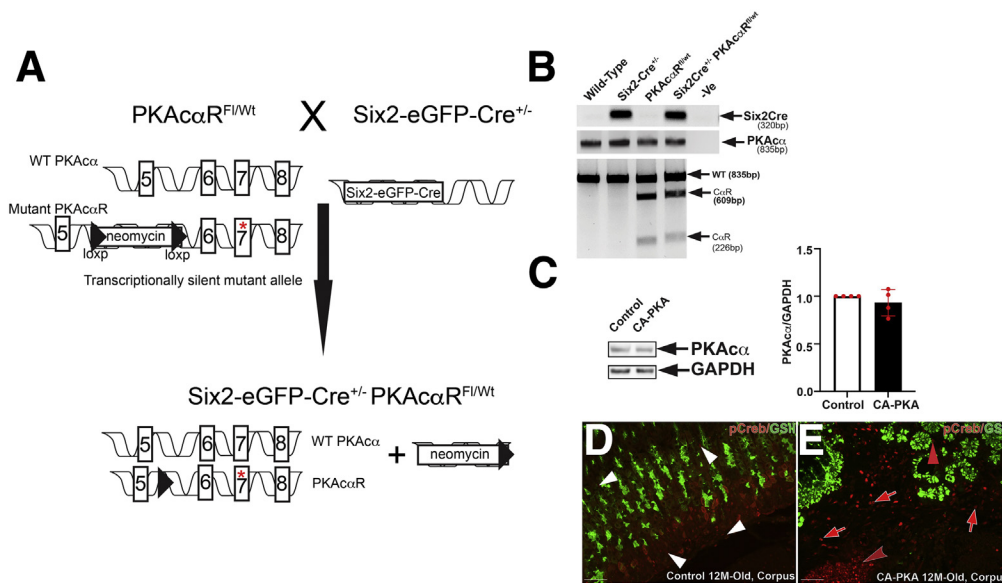


**Figure 1. Generation and characterization of CA-PKA mice.** **A**, A schematic of the genetic construct and mating scheme of the CA-PKA mice.<sup>23</sup> **B**, The presence of the Cre transgene was detected by a polymerase chain reaction that generated a band of 320 bp. For detecting the floxed *Prkaca* allele, a 2-step genotyping protocol was used. First, an 835 bp segment of *Prkaca* was amplified from the tail DNA from all possible genotypes. In mice carrying the mutant floxed allele, the 835bp polymerase chain reaction product was partially digested and generated 609 bp and 226 bp fragments due to the presence of a unique restriction site for the enzyme *Mlu*. **C**, Representative immunoblot and quantification graph showing relative PKA $\alpha$  levels in the mutant corpus vs control ( $n = 4$ ). **D**, Images of corpus sections of 12-month-old control and CA-PKA mice co-stained with p-CREB (PKA activity) antiserum (red) and GSII-lectin (green, mucous neck cells). In control corpus, nuclear p-CREB signal was observed primarily in stromal cells (white arrowheads). In mutant corpus, stronger nuclear p-CREB signal was observed in mutant stromal cells vs control (red arrows), and the number of p-CREB<sup>+</sup> stromal cells were also increased (red arrows). Infiltrated inflammatory cells that either formed tertiary follicles (red concave arrowhead) or scattered in the submucosa also were also strongly positive for p-CREB.; p-CREB signal was also observed in a subset of GSII<sup>+</sup> cells in the mutant (red arrowhead). Scale bars = 50  $\mu$ m.

## Results

We generated and characterized *Six2Cre<sup>+/-</sup>-PKA $\alpha$ R<sup>fl/wt</sup>* (CA-PKA) mice in which *Six2-Cre* activates PKA $\alpha$ R expression (Figure 1, A–E). In PKA $\alpha$ R mutant, a mis-sense mutation hampers its ability to bind with regulatory subunit, leading to constitutive activation.<sup>23</sup> The constitutively active mutant allele is functionally silent, due to the insertion of a floxed neomycin cassette between exons 5 and 6 that prevents transcription in the absence of Cre.<sup>23</sup> Cre-mediated recombination excises the neomycin cassette, and the mutant allele can be transcribed under the endogenous *Prkaca* promoter. Accordingly, no significant change in PKA $\alpha$  levels was detected in the stomach samples of CA-PKA mutants vs control by immunoblotting (Figure 1, C). To determine whether a single-allele mediated expression of constitutively active PKA $\alpha$ R altered PKA activity, we analyzed expression of phospho-CREB (a well-characterized substrate and mediator of cAMP/PKA signaling).<sup>28,29</sup> Immunofluorescence (IF) studies revealed that number of p-CREB<sup>+</sup> cells and intensity of staining were increased primarily in the mesenchymal compartment of the CA-PKA mutant stomach vs control (Figure 1, D–E). Notably, Cre recombinase expression in our CA-PKA mice is driven by the promoter of *Six2* gene that is expressed in the mesenchymal cells of the kidney and stomach.<sup>24,30</sup> It is known that *Six2-Cre* induces recombination in the kidney and stomach; however, in the stomach, *Six2-Cre* activity has not been fully

characterized.<sup>31</sup> To analyze spatiotemporal activity of *Six2-Cre* in the stomach, *Six2-Cre<sup>+/-</sup>-R-tTomato<sup>fl/wt</sup>* mice were generated in which *Six2<sup>+</sup>* cells and their derivatives were labeled permanently with tdTomato (Figure 2, A–B). Stomach sections from newborn *Six2-Cre<sup>+/-</sup>-R-tTomato<sup>fl/wt</sup>* mice were co-stained with red fluorescent protein (RFP) antibody (that detects tdTomato) and either E-cadherin, an epithelial marker, or ACTA2, a mesenchymal marker (Figure 3, A–L). RFP/ACTA2 co-IF revealed that RFP staining overlapped with ACTA2 staining in the gastric mesenchymal compartment, indicating that *Six2-Cre* drives tdTomato expression in the stomach mesenchyme. No RFP signal was detectable in the ECAD<sup>+</sup> epithelial compartment (Figure 3, G–L). These results show that *Six2-Cre* activity in the stomach is restricted to the mesenchymal compartment.

## Gross and Histological Examination

Grossly, the stomach of 6-week-old mutants appeared to be normal; however, 8- to 13-month-old mutants showed marked cystic enlargement of the corpus, and the antrum was mildly enlarged (Figure 4, A–D). Histologically, 6-week-old mutant showed increased height of the corpus mucosa, decreased number of parietal cells and an increase in mucous cells (Figure 4, E–G). The number of pit cells on the surface and basophilic chief cells at the base of the gastric glands were decreased. We observed cystic glands that frequently penetrated the muscularis mucosa into the

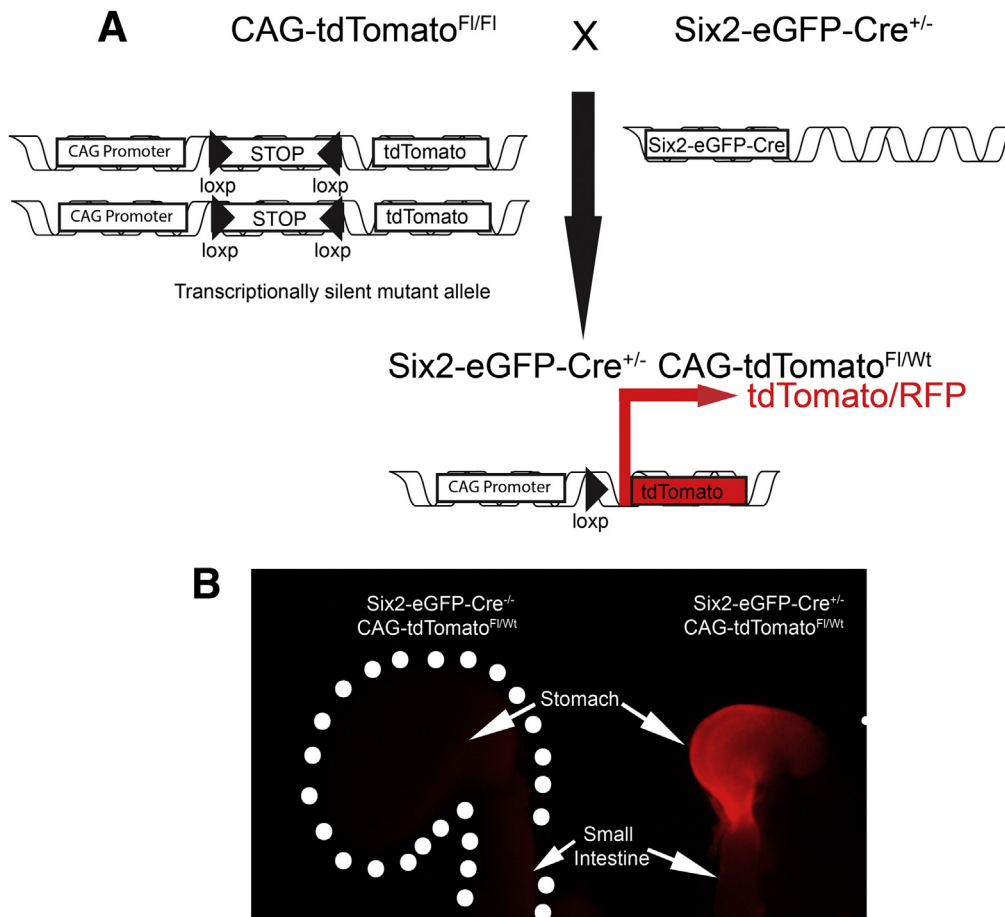


**Figure 2. Generation and characterization of Six2-Cre<sup>+/-</sup>R-tdTomato<sup>fl/wt</sup> mice.** A, A schematic of the genetic construct and mating scheme to generate Six2-Cre<sup>+/-</sup>R-tdTomato<sup>fl/wt</sup>. B, Gross fluorescent image of the stomach from a neonatal control Six2-Cre<sup>-/-</sup>R-tdTomato<sup>fl/wt</sup> stomach (boundary shown with a dotted line) did not show any red fluorescence, whereas Six2-Cre<sup>+/-</sup>R-tdTomato<sup>fl/wt</sup> showed strong td-Tomato fluorescence, specifically in the stomach.

submucosa (not shown). Multifocal submucosal expansion, especially at the border of corpus and antrum, was observed with infiltrating inflammatory cells that were predominantly neutrophils (Figure 4, G). By 12 months of age, the defects increased in severity (Figure 4, H–J). Parietal cells were dramatically reduced, and there was striking mucous neck cell hyperplasia. Mucosa was markedly hyperplastic, inundated with glandular cysts lined by mucous neck cells and contained either none or a few remaining parietal cells. Glands showed severe cystic dilations that frequently penetrated deep into the expanded submucosa and lacked chief cells. Mucosal glands were dysplastic, with epithelial cells showing pleomorphism, nuclear stratification, and loss of polarity. The submucosa was markedly expanded and infiltrated with predominantly mononuclear inflammatory cells that frequently formed large lymphoid aggregates (Figure 4, J). The corpus defects were fully penetrant, and no mutants survived beyond 12 to 14 months of age. Control mice analyzed at similar timepoints did not show any of the defects. Antrum defects were comparatively milder but included multifocal hyperplasia with small cystic dilations in all 12-month-old mutants (Figure 4, K–M). Marked antral hyperplasia and invasive cystic glands with scattered presence of a few goblet cells was observed in 20% of the mutant mice (Figure 4, M).

### Cellular Alterations in CA-PKA Stomach

To visualize mucosal cellular alternations, stomach sections from 6-week-old and 12-month-old control and mutant mice were stained with lectins UEA1 and GSII (Figure 5, A–D). In the control stomach, UEA1-lectin signal was observed specifically in pit cells whereas, GSII-lectin stained mucous neck cells with only a rare overlap. In contrast, UEA1 staining in pit cell layers of 6-week-old mutants was decreased, and aberrant UEA1 staining was observed in deeper regions of gastric glands in GSII<sup>+</sup> cells. Reduced UEA1 staining could indicate either decreased mucus production or fewer pit cells, whereas UEA1/GSII double-positive cells could indicate mucous cell metaplasia. Twelve-month-old mutant mice showed a marked decrease in UEA1-stained pit cells, whereas the gastric glands containing UEA1/GSII-double positive cells were abundant. To determine whether UEA1<sup>+</sup>/GSII<sup>+</sup> cells could be indicative of mucous cell metaplasia, control and mutant stomach sections were co-stained with MUC5B/GSII (Figure 5, E–F). In the control corpus, MUC5B stained a distinct GSII<sup>+</sup> population, but in the mutant, MUC5B/GSII double-positive cells were abundant, an indication of mucous cell metaplasia. To confirm cellular alterations, extracts prepared from the corpus of 8- to 12-month-old control and mutants were analyzed by immunoblotting

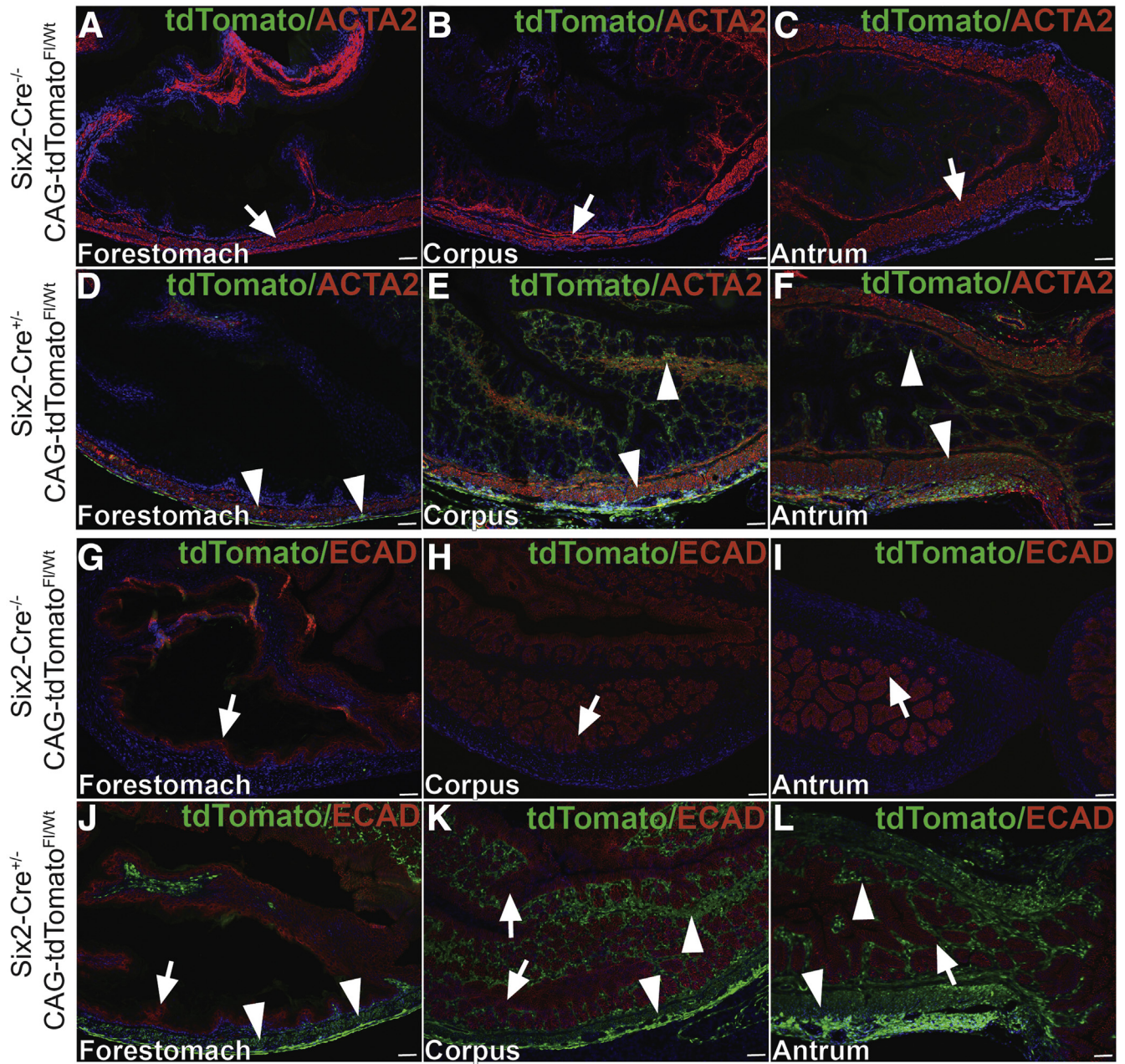


**Figure 3.** Six2-Cre driven tdTomato expression is restricted to the mesenchymal compartment of all 3 regions of the stomach. A–F, Images of 3 regions of stomach from neonatal control and CA-PKA mice co-stained with antisera against RFP (green) and alpha smooth muscle actin (ACTA2) (red); nuclei are stained with DAPI. In the forestomach (A), corpus (B), and antrum (C) regions of control Six2-Cre<sup>-/-</sup>R-tdTomato<sup>fl/wt</sup> stomach, no RFP signal was observed; ACTA2-stained mesenchymal cells of all 3 stomach regions are indicated (arrows). In Six2-Cre<sup>+/-</sup>R-tdTomato<sup>fl/wt</sup> stomach (D–F), RFP signal observed in the lamina propria submucosa, muscularis mucosae, and muscularis externa of stomach (arrowheads) overlapped almost completely ACTA2-stained cells of all 3 stomach regions. G–L, Images of 3 regions of stomach from neonatal control and CA-PKA mice co-stained with antisera against RFP (green) and ECAD (red); nuclei are stained with DAPI. In the forestomach (G), corpus (H), and antrum (I) regions of control Six2-Cre<sup>-/-</sup>R-tdTomato<sup>fl/wt</sup> stomach, no RFP signal was observed; ECAD-stained epithelial cells of all 3 stomach regions are indicated (arrows). In Six2-Cre<sup>+/-</sup>R-tdTomato<sup>fl/wt</sup> stomach (J–L) RFP signal in the lamina propria (arrowheads) and developing muscularis externa (arrowheads) is indicated; no RFP signal (green) was observed in ECAD-stained epithelial cells of all 3 stomach regions (arrows). Scale bars = 50  $\mu$ m

(Figure 5, G) with antisera against gastrin (a pit cell marker), TFF2 (a mucous neck cell marker), and MUC5B. In mutants, gastrin protein levels were reproducibly lower, whereas TFF2 and MUC5B levels

were consistently higher. Together, these results show that CA-PKA mutant stomachs have pit cell hypoplasia and mucous neck cell hyperplasia with metaplastic changes.

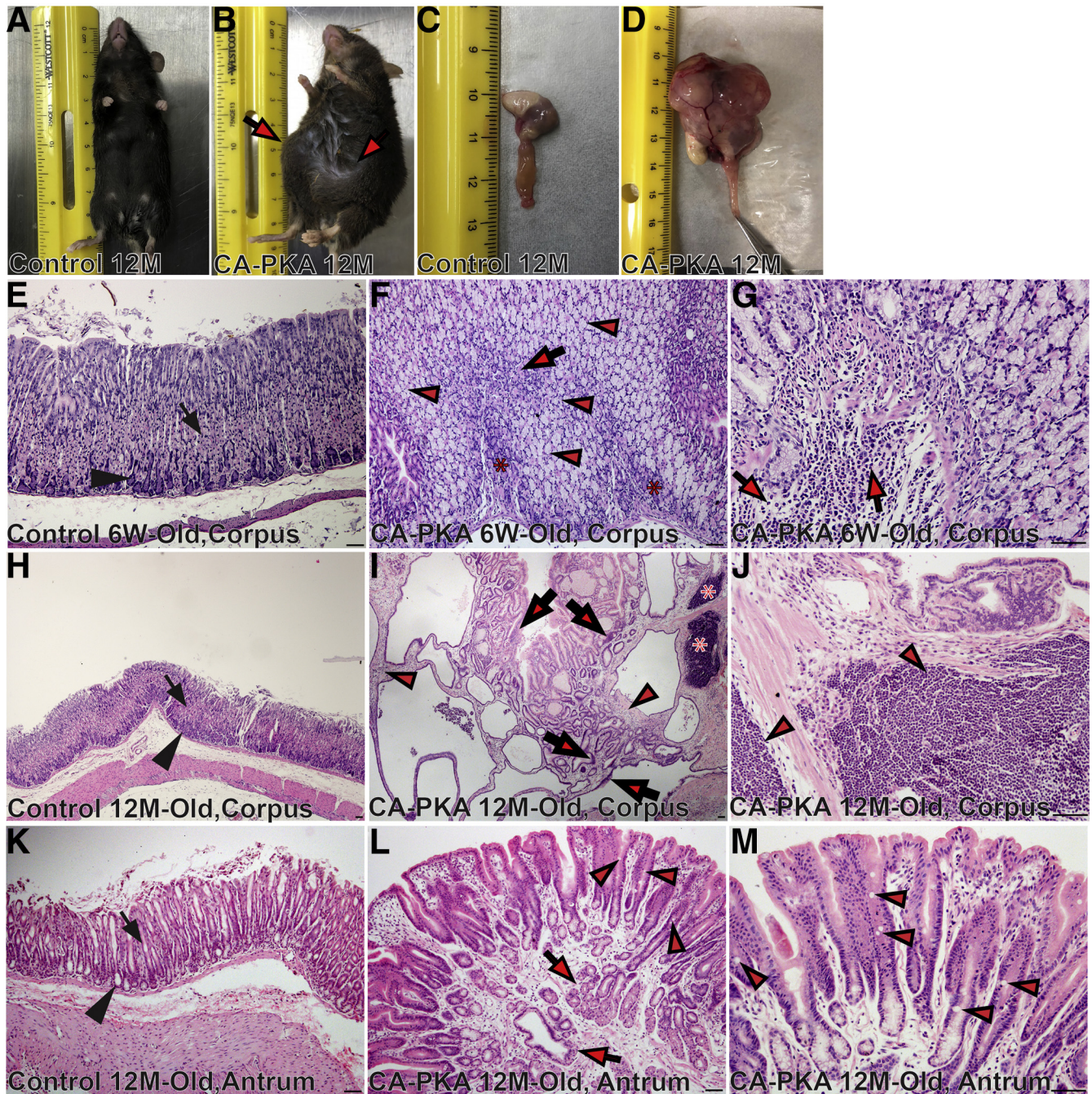


**Figure 4. CA-PKA mice show gastric mucosal maldevelopment and develop preneoplastic lesions.** A–D, Images of 12-month-old normal control (A) and CA-PKA mouse (B) with abdominal enlargement (arrows). Gross morphology of normal control (C) and mutant stomach (D) with marked enlargement. E–M, Hematoxylin and eosin-stained images of the stomach from 6-week-old and 12-month-old control and CA-PKA mice. In 6-week-old and 12-month-old control corpus (E & H), parietal (arrow) and chief cells (arrowhead) are indicated. F, Six-week-old mutant corpus with remaining parietal (arrow), chief cells (asterisks), and mucous cell hyperplasia (arrowheads) is shown. G, Image shows infiltrating neutrophils in the CA-PKA corpus (arrows). I, Twelve-month-old CA-PKA corpus showing stromal expansion (arrowheads), cystic dysplasia with nuclear stratification (arrows), and lymphocytic infiltration (asterisks). J, Lymphocytic infiltration (arrowheads) in 12-month-old mutants. K, Antrum from a 12-month-old control mouse showing the neck (arrow) and base (arrowhead) of antral glands. L, Mutant antrum showing invading antral glands (arrows) and goblet cells (arrowheads). M, Goblet cells (arrowheads) in 12-month-old mutants. Scale bars = 50  $\mu$ m.

To determine whether there are alterations in parietal and chief cells, stomach sections were co-stained with DBA and MIST1 that label parietal and chief cells, respectively

(Figure 5, H–K). Six-week-old and 12-month-old control stomach showed a robust population of DBA<sup>+</sup> and MIST1<sup>+</sup> cells. In contrast, there were fewer DBA<sup>+</sup> parietal cells and

MIST1<sup>+</sup> chief cells in 6-week-old mutants. In 12-month-old mutant stomachs, there was a further striking reduction in DBA<sup>+</sup> parietal cells, and MIST1 expressing cells were rare. To further analyze parietal cell loss, expression of parietal cell maker ATP4A was analyzed by co-IF (Figure 5, L–M) and immunoblotting (Figure 5, N). Co-IF analysis showed scant presence of ATP4A<sup>+</sup> cells, and immunoblots revealed weak to undetectable levels of ATP4A and undetectable MIST1 expression (Figure 5, M–N) in the mutant. Together, these results demonstrate severely reduced parietal cells and the loss of expression of MIST1 in chief cells of the CA-PKA mutants. Because endocrine cells regulate the growth of gastric mucosa, the number of endocrine cells in stomach sections from control and mutant mice were assessed by co-staining with chromogranin A (CHGA) (a pan endocrine cell marker) (Figure 6, A–H).<sup>32</sup> The number of CHGA<sup>+</sup> cells was similar in both corpus and antrum of 6-week-old control and mutant samples, but the number of CHGA<sup>+</sup> cells decreased in the mutant corpus at 12-month-old timepoint.

### Gastric SPEM and SPEM With Intestinal Characteristics

Atrophic gastritis characterized by parietal and chief cell atrophy is a precursor lesion to SPEM and intestinal metaplasia.<sup>33</sup> SPEM in the mutant stomach was observed in both 6-week-old (not shown) and 12-month-old mutants as TFF2<sup>+</sup>/GSII<sup>+</sup> cells were detected in the basal corpus glands, present just above the mesenchyme or invading into the mesenchyme (Figure 7, A–F). Co-labeling of corpus glands with differentiated chief cell marker, gastric intrinsic factor (GIF), and any mucous cell marker is considered strong evidence of SPEM.<sup>33</sup> In 6-week-old mutants, GIF/GSII double-positive cells were frequently observed in the mutant corpus, and some of these glands containing these cells were cystic and invaded into the submucosa (Figure 7, G–L). In 12-month-old mutants, large cystic glands that contained GIF/GSII double-positive cells were abundant (Figure 7, M–R). Together, these results indicate that mutant corpus glands undergo SPEM.

To determine whether mutant gastric mucosa acquired intestinal characteristics, periodic acid-Schiff (PAS) PAS/Alcian blue (AB) staining was performed (Figure 8, A–H). Pit cells in the control stomach showed magenta color following PAS/AB staining, indicating the presence of neutral mucins; staining of a serial section with AB did not show any staining, confirming the absence of acid mucins. In contrast, pit cells and a subset of mucous cells in the CA-PKA corpus stomach stained dark blue with PAS/AB and light blue with AB alone, indicating the presence of acid mucins. As acid mucins are normally present in the intestine, these results indicate that CA-PKA corpus gastric mucosa has acquired intestinal characteristics. Furthermore, we analyzed the expression of villin1 (Figure 8, I–N), which is induced in atrophic human and mouse stomach following *H. Pylori* infection and is indicative of intestinal metaplasia.<sup>34</sup> Co-IF analysis showed that strong villin1 expression is induced in the glandular cells of mutant corpus; in contrast, Villin1<sup>+</sup> cells were rarely observed in the control corpus stomach.

We also analyzed the expression of polymeric immunoglobulin receptor (PIGR) because its levels increase in intestinal metaplasia (Figure 8, O).<sup>35</sup> Immunoblotting showed that mutant stomach had dramatic upregulation of PIGR vs control. Although a dramatic upregulation of VIL1 and PIGR has been reported in intestinal metaplasia, these markers are expressed in low amounts in normal gastric mucosa, and their increased expression as definitive evidence of intestinal metaplasia is debatable.<sup>33,35,36</sup> Expression of MUC2, a marker of differentiated intestinal mucous cell, in the stomach is well-accepted as a marker of intestinal characteristics/metaplasia.<sup>33</sup> Therefore, we stained control and CA-PKA stomach sections with MUC2 antiserum and found that a subset of mucous cells lining cystic gastric glands of CA-PKA corpus mucosa showed strong expression of MUC2, whereas control corpus mucosa did not show any detectable MUC2 signal. Together, these results show that the corpus mucosa of CA-PKA stomach acquired intestinal characteristics (Figure 8, P–S).

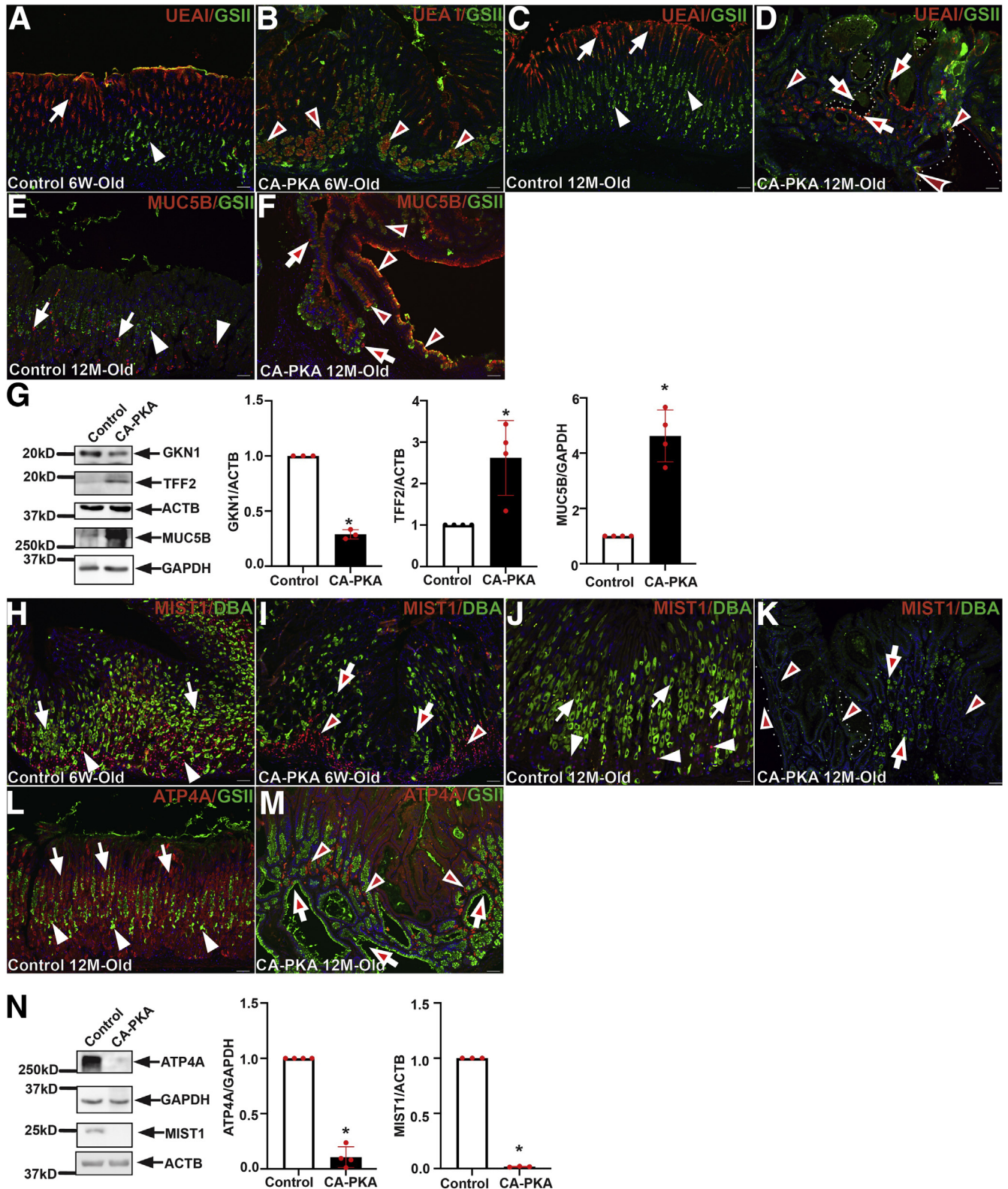
Presence of goblet cells is one of the key features of intestinal metaplasia.<sup>33</sup> Although we rarely observed cells with characteristic intestinal goblet cell morphology in the mutant corpus, PAS/AB staining of the mutant antrum indicated the presence of goblet cells in the neck region of antral glands (Figure 8, T–A'). IF analysis showed that a subset of mucous cells (with characteristic goblet cell morphology) in antral glands of CA-PKA showed expression of MUC2 confirming intestinalization/intestinal metaplasia of the antral mucosa in CA-PKA stomach. (Figure 8, B'–E').

### mRNA Sequencing Analysis

To determine the molecular signature of the observed phenotype of atrophic gastritis with expanded stromal and epithelial compartments, we compared transcriptomes of corpus of 7- to 8-month-old control (n = 4) and mutant (n = 4) mice by mRNA sequencing (mRNA seq). Of 27114 mRNAs detected, 4893 were found to be differentially expressed (2397 upregulated and 2496 downregulated padj < 0.05 and Log2 fold change > 0) (Figure 9, A–B). Gene Ontology (GO) analyses of significantly upregulated mRNAs identified the top 20 categories as being related to immune function. The top 20 categories for downregulated mRNAs were related to metabolism and oxidative phosphorylation (Figure 9, C–D). Many similar categories were identified using Kyoto Encyclopedia of Genes and Genomes and Reactome pathway analyses (Figure 10, A–B). mRNA seq analysis revealed a decrease in the expression levels of genes known to be enriched and/or specifically expressed in parietal cells or chief cells supporting a decrease in their number (Figure 11, A–B).<sup>35,37</sup> Over-representation of categories representing metabolism in the analysis of downregulated mRNAs is also likely indicative of parietal cell loss because a relatively large proportion of parietal cells transcriptome represents genes involved in various forms of cellular metabolism due to their energy-intensive acid secretory function.<sup>38,39</sup> We also observed increased expression of mRNAs enriched in mucous neck and tuft cells, whereas pit cell and endocrine cell marker genes were

decreased (Figure 11, A-C).<sup>37</sup> Together, these results confirm alterations in the stomach differentiated cell populations. The mutant corpus showed increased levels of multiple canonical SPEM transcripts *Cftr*, *Pigr*, *Muc13*,

*Dmbt1*, *Wfdc2*, *Gda*, *Clu*, *Plaur*, *Slc5a1*, and *Lgals4* (Figure 11, D), as observed previously in multiple models of gastric cancer.<sup>35,40-43</sup> We confirmed upregulation of protein levels of VIL1, PIGR, and CD44 in our model. Gastric stem or





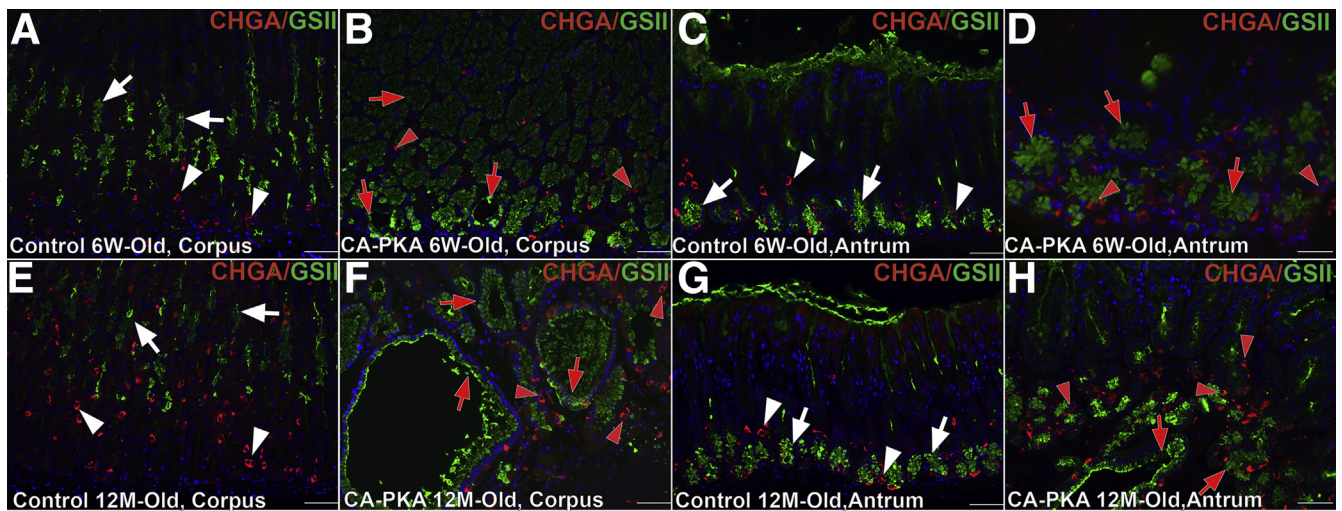


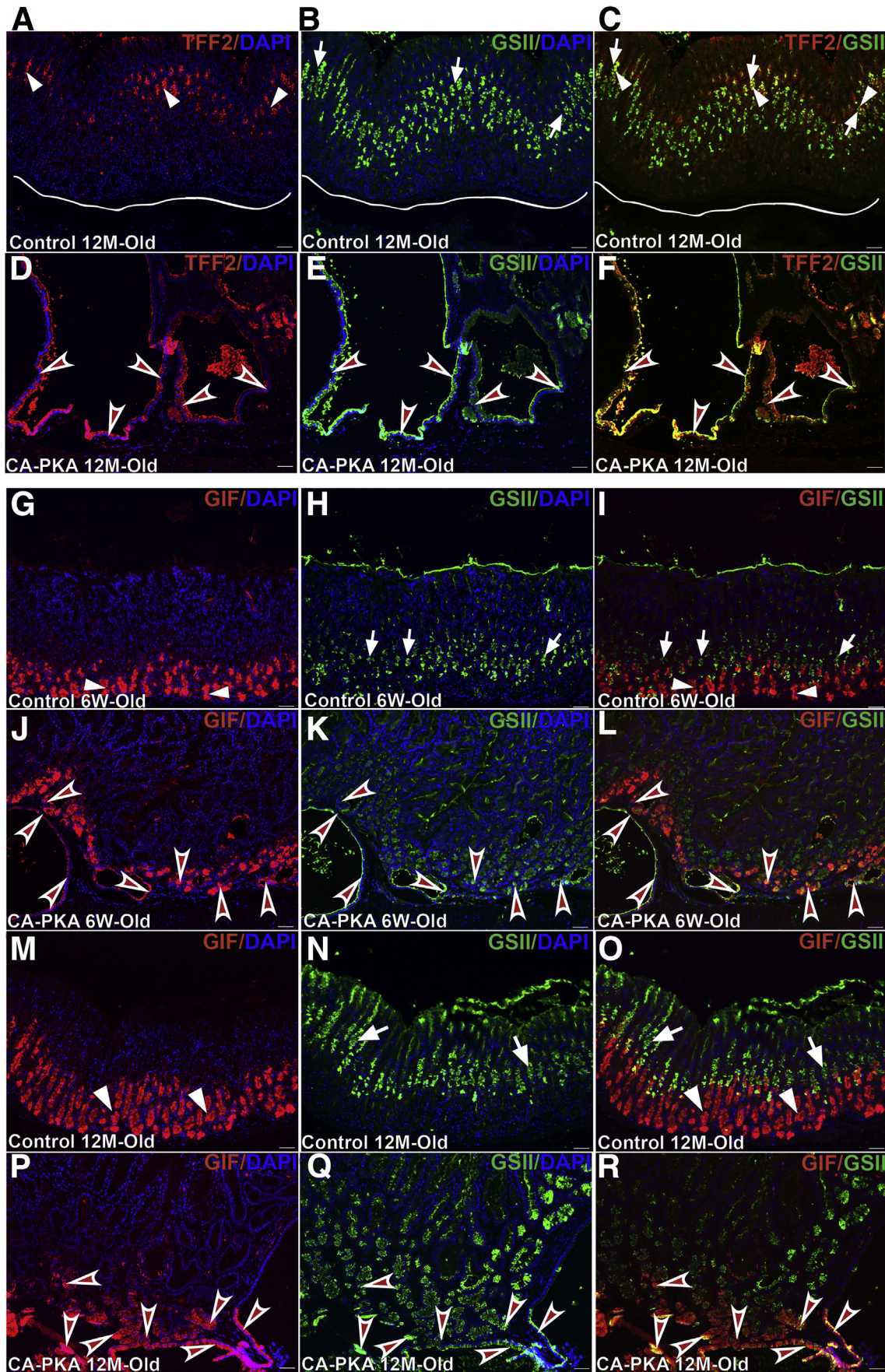
**Figure 6.** Alterations occur in endocrine cells in CA-PKA corpus A–H, Images of corpus and antrum sections from 6-week- and 12-month-old control and CA-PKA mice co-stained with pan-endocrine cell marker chromogranin A (CHGA) (red) and GSII-lectin (green). In the corpus (A) and antrum (C) of 6-week-old control mice, CHGA<sup>+</sup> (white arrowhead) and GSII<sup>+</sup> (white arrow) cells are indicated. In the corpus (B) and antrum (D) of 6-week-old mutants, the CHGA population (red arrowheads) was unaffected, whereas hyperplasia of GSII<sup>+</sup> (red arrows) (in mutant corpus) can be seen. In the corpus (E) of 12-month-old control mice, CHGA<sup>+</sup> (white arrowhead) and GSII<sup>+</sup> (white arrow) cells are indicated. In the corpus of 12-month-old CA-PKA mice (F) CHGA<sup>+</sup> (red arrows) population was decreased. In the antrum (G) of 12-month-old control mice, CHGA<sup>+</sup> (white arrowhead) and GSII<sup>+</sup> (white arrow) cells are indicated. In the antrum (H) of 12-month-old mutants, the CHGA<sup>+</sup> population (red arrowheads) was unaffected. Scale bars = 50  $\mu$ m.

progenitor cells have been proposed to be candidates for cancer stem cells, a possible source of cancer initiation.<sup>44,45</sup> Similarly, we observed upregulation of various gastric and cancer stem cell markers (Figure 11, D).<sup>35</sup> Together, mRNA seq results show that CA-PKA stomach shows a molecular signature of SPEM with intestinal characteristics.

GO analysis showed that upregulated genes had categories almost exclusively involved in immune pathways activation, including the innate, adaptive immune system, and cytokine-mediated signaling pathways (Figure 12, A–E). Multiple genes encoding chemokines, cytokines, and their receptors showed dramatic upregulation (Figure 12, C–E). Many of these differentially expressed mRNAs have been implicated in inflammation, polyps, and carcinogenesis of stomach and could be secreted by stromal, epithelial, or inflammatory cell compartments.<sup>46–48</sup> To identify

inflammatory cell types possibly recruited by and/or contributing to this inflammatory milieu, we searched lineage specific markers in the mRNA seq data. Myeloid-derived suppressor cells have been implicated in atrophic gastritis and SPEM and gastric cancer pathogenesis by inhibiting T-cell responses against tumor cells.<sup>49</sup> We identified multiple markers of myeloid-derived suppressor cells including *Arg1* (Figure 12, F). Co-staining of control and mutant stomach with ARG1 and GSII showed increased infiltration of ARG1<sup>+</sup> cells (Figure 12, G–H). T-cell receptor components such as transcripts encoding CD3 subunits and TCR $\gamma$  were identified (Figure 12, F). Co-staining confirmed marked infiltration of CD3<sup>+</sup> T-cells in the mutant corpus (Figure 12, I–J). Of the identified cytokines, IL11 and IL1 have been implicated to stimulate STAT3 signaling in gastric preneoplasia, adenocarcinoma, and Peutz-Jeghers Syndrome (PJS).<sup>48,50,51</sup> We

**Figure 5.** (See previous page). Cellular alterations in CA-PKA mutant stomach. A–D, Stomach from 6-week- and 12-month-old control and CA-PKA mice co-stained with lectins UEA1 (red) and GSII (green). In control (A, C), UEA1 in pit cells (arrows) and GSII signal in mucous neck cells (arrowheads) are shown. In mutant (B, D) UEA1/GSII double-positive cells (arrowheads) and cystic glands (dotted lines) containing both UEA1<sup>+</sup> and GSII<sup>+</sup> cells (arrows) are shown. E–F, Stomach from 12-month-old control (E) and CA-PKA (F) mice co-stained with MUC5B (red) and GSII-lectin (green). In control, MUC5B (arrows) and GSII (arrowheads) stained distinct cells. In the CA-PKA corpus, increased MUC5B/GSII double-positive cells (arrowheads) and remaining MUC5B<sup>+</sup>/GSII<sup>−</sup> cells (arrows) are shown. G, Representative immunoblots and quantification graphs (\**P* < .05) showing gastrin (n = 3), TFF2 (n = 4), and MUC5B (n = 4) relative levels in corpus extracts of control and CA-PKA mice. H–K, Stomach from control and CA-PKA mutant co-stained with MIST1 (red) and DBA-lectin (green). In controls (H, J), MIST1<sup>+</sup> chief cells (arrowheads) and DBA<sup>+</sup> parietal cells (arrows) are shown. In 6-week-old mutant (I) DBA<sup>+</sup> (arrows) and MIST1<sup>+</sup> cells (arrowheads) were fewer. In 12-month-old mutant (K), glands containing severely reduced (arrows) or no DBA<sup>+</sup> cells (arrowheads) are indicated. L–M, Stomach sections from control and mutant co-stained with parietal cell marker, ATP4A (red, arrows) and GSII-lectin (green, arrowheads). In control (L) ATP4A<sup>+</sup> (arrows) and GSII<sup>+</sup> (arrowheads) cells are indicated. Mutant glands (M) containing severely reduced (arrowheads) or no ATP4A<sup>+</sup> cells (arrows) are indicated. N, Representative immunoblots and quantification graphs (\**P* < .05) showing ATP4A (n = 4) and MIST1 (n = 3) relative levels in mutant corpus vs control. Scale bars = 50  $\mu$ m. Blue (DAPI).



determined that STAT3 signaling is upregulated, as we observed marked increase in levels of p-STAT3(T705) in the epithelial cells, stromal cells, and infiltrated inflammatory cells of both corpus and antral regions of mutants, whereas no signal was observed in the control stomach (Figure 12, K–N).

### Increased Growth Factors and Proliferation

To assess alternations in proliferation, immunostaining with the proliferation marker PCNA was performed (Figure 13, A–H). In 6-week- and 12-month-old control mice, the proliferation zones in the corpus and antrum were restricted to the isthmus. In contrast, in the mutant corpus, proliferation zone was expanded, and PCNA<sup>+</sup> cells were also increased in the mesenchyme; mutant antrum also showed extended proliferation zone, and PCNA<sup>+</sup> cells were also observed in the expanded GSII<sup>+</sup> antral gland base. In 12-month-old mutant corpus, the proliferation center was markedly expanded beyond the isthmus, and PCNA<sup>+</sup> cells were observed in multi-layers in cystic glands. Immunoblotting confirmed marked increase in the PCNA levels in the corpus extracts of mutants vs. control (Figure 13, I). Furthermore, mRNA seq analysis identified upregulation of multiple growth factors genes in mutant vs control mice that could be driving proliferation (Figure 13, J). During SPEM, chief cells in the basal regions are known to undergo dedifferentiation and enter cell cycle via increased expression of SOX9 and CD44.<sup>52</sup> Co-IF analysis showed marked increase in the number of SOX9<sup>+</sup> cells in corpus and antral regions of mutant vs control (Figure 13, L–O). mRNA seq analysis also showed increased levels of SOX9 and CD44 (Figure 11, D), and immunoblotting confirmed increased CD44 levels in the mutant (Figure 13, J). To assess alternations in apoptosis, immunostaining with the apoptosis marker cleaved caspase-3 was performed. IF analysis did not show any differences in the number of caspase-3 in mutant vs control stomach (not shown). However, mRNA seq identified multiple genes implicated in pyroptosis and necroptosis (Figure 13, K).

### Mis-regulation of BMP and ERK Signaling

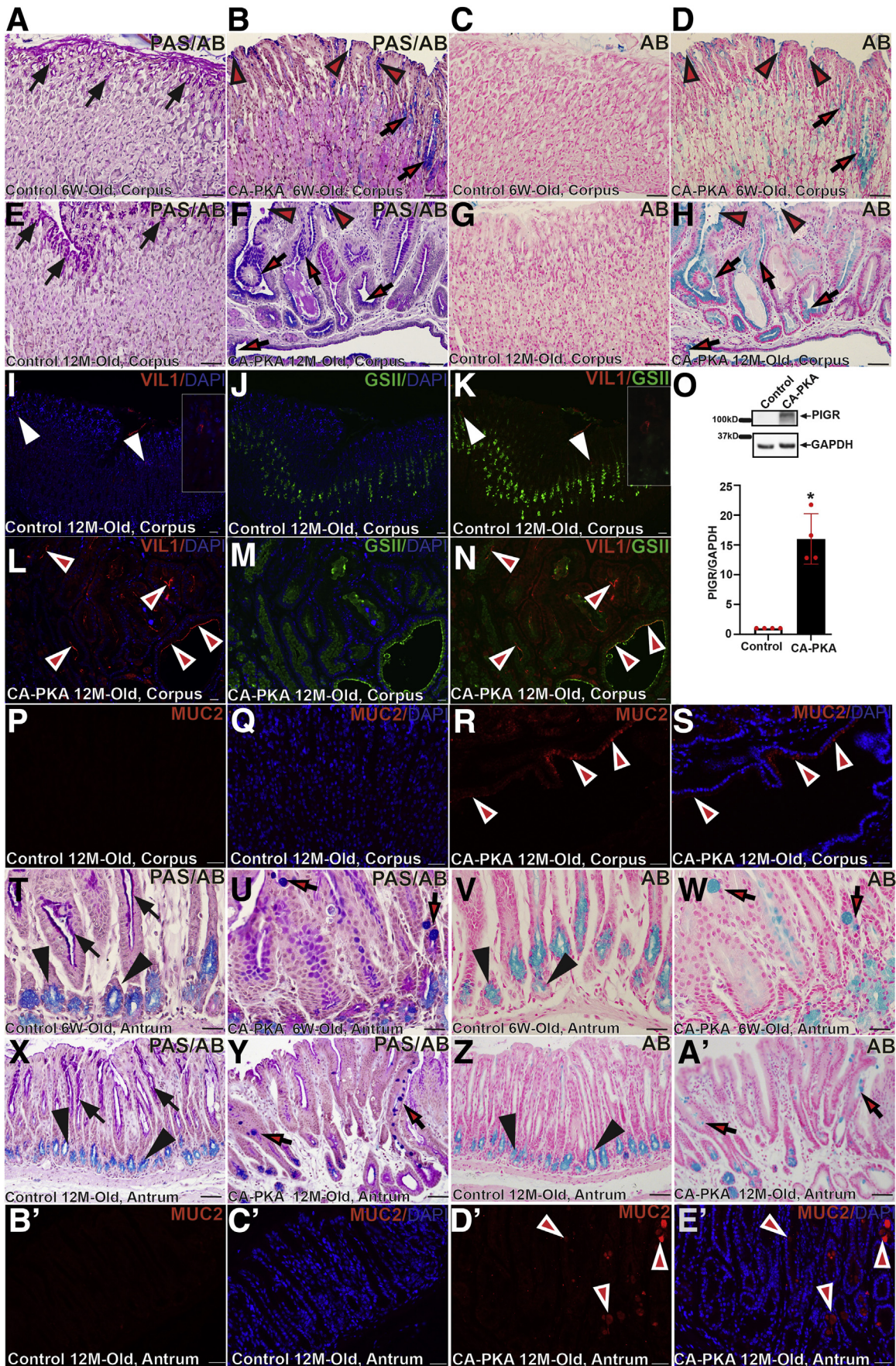
One of the key mechanisms that regulates inflammation and the size of epithelial-stromal compartments in the stomach is BMP signaling.<sup>2,6</sup> mRNA seq analysis showed marked alterations in multiple components of BMP pathway (Figure 14, A). BMP ligands (*Bmp3*, *Bmp4*), BMP receptor (*Bmpr1b*), receptor *Smad9*, and target transcription factors (*Id4* and *Id2*) were downregulated. Most remarkably, there was marked upregulation of a BMP antagonist, gremlin 1 (*Grem1*). Further, immunoblotting analysis confirmed that

gremlin 1 levels were consistency upregulated in corpus extracts of mutant vs control (Figure 14, B). Gremlin 1 is a well-established inhibitor of BMP signaling.<sup>53</sup> To determine the activation status of BMP signaling, we analyzed the levels of phosphorylated SMAD1/5 by immunoblotting. We found that phospho-SMAD1/5 signal was reduced in the mutant corpus vs control, indicating reduced BMP pathway activity in the mutant (Figure 14, B). Co-IF analysis, with phospho-SMAD1/5/9 antibody, also showed a decrease in the level of activated receptor SMADs in both epithelial and stromal compartments of the mutant stomach vs control (Figure 14, C–H). Together, these results suggest that stromal PKAcαR expression stimulates epithelial hyperproliferation, inflammation, and associated preneoplastic lesions at least partly by inhibiting BMP signaling.<sup>16</sup> We also analyzed ERK signaling as it is one of the major regulators of cellular proliferation in the stomach and PKA crosstalks and activates MAPK signaling.<sup>16</sup> Immunoblotting revealed that phospho-ERK levels were upregulated in mutant corpus in comparison to control (Figure 14, I). Further co-IF analysis of corpus stomach revealed the p-ERK activation is predominantly localized to the mesenchymal compartment of the mutant corpus (Figure 14, J–O).

### Characterization of Stromal Cell Population

Recently, a distinct population of gastric stromal cells was shown to be located underneath the gland base that secretes BMP antagonists, including gremlin 1 and these stromal cells expressed mesenchymal markers ACTA2 and MYH11.<sup>11</sup> To characterize mesenchymal cell population that drives the gastric pathology in CA-PKA mice, we generated Six2-Cre<sup>+/-</sup>-PKAcαR<sup>fl/wt</sup>;R-tdTomato<sup>fl/wt</sup> mice in which Six2<sup>+</sup> progenitor-derived cells containing PKAcαR allele are permanently labeled with tdTomato. To characterize this mesenchymal cell population, we performed Co-IF on stomach sections from 8M-old Six2-Cre<sup>+/-</sup>-PKAcαR<sup>fl/wt</sup>;R-tdTomato<sup>fl/wt</sup> (mutant) and Six2-Cre<sup>+/-</sup>;PKA<sup>wt/wt</sup>;R-tdTomato<sup>fl/wt</sup> (control) mice with RFP antiserum (that stains tdTomato) and either antisera against ACTA2, vimentin (VIM), or platelet-derived growth factor receptor alpha (PDGFRA), markers that are expressed by gastric stromal cells (Figure 15, A–R).<sup>54,55</sup> Signals for RFP and all 3 stromal markers were specifically localized to the mesenchymal compartment of the control and mutant stomach. In mutant corpus, the stromal population identified by all 4 markers was markedly expanded vs control. In control, ACTA2 expression largely overlapped with RFP expression in stromal cells near the gland base, muscularis mucosae, and in between glands. A relatively small RFP<sup>+</sup>/ACTA2<sup>-</sup> population was also detected in the stomach (Figure 15, A–C),<sup>54</sup>

**Figure 7. (See previous page). SPEM develops in CA-PKA corpus.** A–F, Stomach sections from 12-month-old control and CA-PKA mice co-stained with TFF2 antiserum (red) and GSII lectin (green). In control (A–C), TFF2<sup>+</sup> (arrowheads) and GSII<sup>+</sup> (arrows) cells were observed away from the gland base (line). In CA-PKA mice (D–F), TFF2<sup>+</sup>/GSII<sup>+</sup> cystic glands (arrowheads) invaded into the submucosa. G–R, Stomach sections from 6-week- and 12-month-old control and CA-PKA mice co-stained with GIF (red, chief cells) and GSII (green, mucous neck cells). In control (G–I, M–O), GIF in chief cells (arrowheads) and GSII signal in mucous neck cells (arrows) is shown. In 6-week-old CA-PKA corpus (J–L) GIF/GSII double-positive cells are present in cystic and non-cystic glands (arrowheads). In 12-month-old CA-PKA mice (P–R), large cystic glands with GIF/GSII double-positive cells (arrowheads) are shown. Scale bars = 50μm. Blue (DAPI).



In mutant corpus, RFP<sup>+</sup>/ACTA2<sup>+</sup> population was highly expanded and localized underneath the infiltrating gland base and in between glands (Figure 15, D–F). Co-IF staining with RFP and VIM in control revealed that VIM expression almost completely overlapped with RFP expression in stromal cells near the gland base, in the muscularis mucosae, and in between glands (Figure 15, G–I). In mutant, the RFP<sup>+</sup>/VIM<sup>+</sup> population was highly expanded and labeled almost all of the stromal cells localized in the infiltrating gland base and in between glands (Figure 15, J–L). Co-IF staining with RFP and another stromal marker PDGFRA in control revealed that stromal cells that coexpressed PDGFRA/RFP were relatively fewer and localized predominantly between glands; additionally, both PDGFRA<sup>+</sup>/RFP<sup>-</sup> and PDGFRA<sup>-</sup>/RFP<sup>+</sup> cell populations were observed (Figure 15, M–O). In the mutant, PDGFRA<sup>+</sup>/RFP<sup>-</sup> cells were expanded and wrapped around the gastric glands, whereas PDGFRA<sup>+</sup>/RFP<sup>+</sup> cells were present in between the expanded stroma and represented a relatively small population of expanded stroma (Figure 15, P–R).

## Discussion

We report a novel role of mesenchymal PKA $\alpha$  in gastric epithelial development and homeostasis maintenance through reciprocal effects on ERK and BMP signaling activity. We find that PKA activity in the gastric mesenchymal compartment must be tightly regulated and demonstrate that the expression of constitutively active PKA $\alpha$ R from a single allele in the gastric mesenchyme nonautonomously disrupts gastric homeostasis by altering epithelial proliferation and development that ultimately causes preneoplastic lesions including atrophic gastritis, SPEM with intestinal characteristics, and dysplastic invasive glands. The preneoplastic lesions occurring in response to PKA $\alpha$ R expression were similar to those caused by infection with *H. pylori*, a primary etiological agent responsible for most gastric cancer cases.<sup>33</sup>

Multiple mechanisms, such as inflammation, impaired BMP signaling, and altered gastrin levels, result in oxyntic atrophy.<sup>2,6,33,56–58</sup> It is known that oxyntic atrophy leads to compensatory hypergastrinemia and that both overexpression and the deletion of the gastrin gene result in

oxyntic atrophy in mice.<sup>5,32,57–60</sup> However, in our model, hypergastrinemia appears to be an unlikely outcome of oxyntic atrophy because hypergastrinemia causes foveolar/pit cell hyperplasia, but CA-PKA mice show foveolar hypoplasia.<sup>33</sup> Gastrin stimulates proliferation of gastric mucosal cells including parietal and ECL cells.<sup>32,61</sup> Notably, RNA seq results from stomachs expressing CA-PKA revealed significantly decreased expression of a pan-endocrine cell marker *Chga* and ECL and D cell-enriched genes. Whether the downregulation of endocrine cell markers represents a decrease in the absolute number of the corpus endocrine cell population remains to be determined. Also, it is not yet known whether reduced numbers of G cells and/or impaired gastrin signaling contribute to decreased parietal cells in CA-PKA mice. Nevertheless, it appears that altered gastrin levels may not be the only factor to cause oxyntic atrophy in CA-PKA mice because 12-week-old gastrin knockout mice have normal gastric histology, whereas decreased parietal cell numbers in CA-PKA mice is obvious at 6 weeks of age.<sup>56</sup> Therefore, additional factors such as inflammation and/or downregulated BMP signaling could be contributors to the relatively early onset of oxyntic atrophy in CA-PKA mice.

Given that chronic inflammation is one of the key drivers of gastric tumors, induction of a potent inflammatory microenvironment by mesenchymal-specific PKA $\alpha$ R was one of the key findings of this study.<sup>46,47,62</sup> These results are highly relevant because gastric stromal cells have been found to be a target of *H. pylori* infection.<sup>11,63</sup> *H. Pylori*-mediated targeting of stromal cells inhibits BMP signaling by upregulating BMP antagonists including gremlin 1 and downregulating BMP ligand BMP2.<sup>11</sup> Inhibition of BMP signaling is known to contribute to epithelial hyperproliferation and inflammation, which can further derive hyperplasia.<sup>4,5,7,11</sup> Our results show that PKA signaling is a key regulator of stromal cell function, and mesenchymal PKA activation leads to inhibition of BMP signaling by altering multiple BMP signaling components, including marked upregulation of BMP antagonist gremlin 1. We also show that in our Six2-Cre<sup>+/+</sup>-PKA $\alpha$ R<sup>fl/wt</sup>;R-tdTomato<sup>fl/wt</sup> mouse model, a subpopulation of tdTomato<sup>+</sup> cells (Six2<sup>+</sup> progenitor-derived stromal cell population containing

**Figure 8.** (See previous page). CA-PKA corpus develops SPEM with intestinal characteristics A–H, Corpus (serial) sections from 6-week- and 12-month-old control and CA-PKA mice stained with PAS and AB or AB alone. PAS/AB staining in control showed normal magenta staining in pit cells of controls (A & E) (arrows), whereas in mutants (B & F), there is aberrant blue staining in pit (arrowheads) and mucous neck cells (arrows). With AB (D & H), similar cells showed light blue staining (arrows and arrowheads). I–N, Stomach sections from 12-month-old control and CA-PKA mice co-stained with villin1 (VIL1) antiserum (red), GSII-lectin (green), and DAPI (blue). In control (I & K), VIL1 (arrowheads and insets) expression was infrequent. In mutant, VIL1<sup>+</sup> cells (arrowheads) were increased. O, Representative immunoblot and quantification graph (\*P < .05) showing relative PIGR levels (n = 4) in the mutant corpus vs control. P–S, Corpus stomach sections from 12-month-old control and CA-PKA mice co-stained with Mucin 2 (MUC2) antiserum (red) and DAPI (blue). In control (P & Q), no MUC2<sup>+</sup> cells were observed. In mutant (R & S), MUC2<sup>+</sup> cells in a cystic gland (arrowheads) are indicated. Antrum sections from 6-week- and 12-month-old control and CA-PKA mice stained with PAS/AB or AB alone. In control (T & X), normal magenta staining in the neck (arrows) and light blue staining (arrowheads) in the base is indicated. In mutants (U & Y), aberrant dark blue staining in goblet cells with PAS/AB staining (arrows) is indicated. With AB, light blue staining (V & Z) in the gland base in control, and in goblet cells of the mutant antrum (W & A') (arrows) is shown. B'–E', Antrum stomach sections from 12-month-old control and CA-PKA mice co-stained with Mucin 2 (MUC2) antiserum (red) and DAPI (blue). In control antrum (B' & C'), no MUC2<sup>+</sup> cells were observed. In mutant (D' & E'), MUC2<sup>+</sup> cells in multiple antral glands (arrowheads) with variable MUC2 expression are indicated. Scale bars = 50  $\mu$ m.

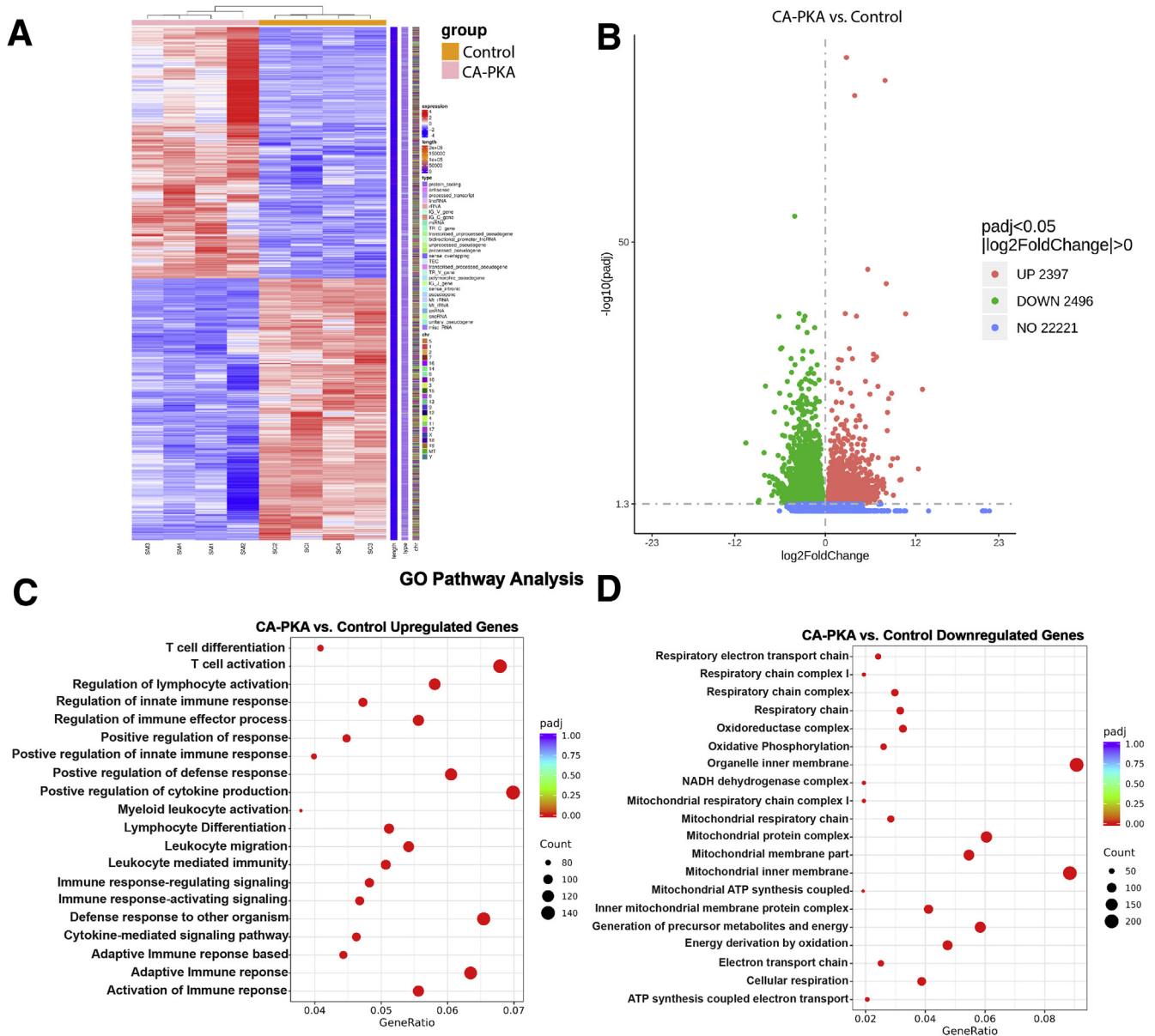


**Figure 9.** mRNA seq and GO analysis of control and CA-PKA corpus identify misregulation of pathways involved in immune response and metabolism (A-D). A, Heatmap of differentially expressed genes in corpus regions of CA-PKA mice vs control identified by mRNA seq analysis. B, Volcano plot of differentially expressed upregulated and downregulated genes in corpus regions of CA-PKA mice vs control identified by mRNA seq analysis. C, Top 20 pathways revealed by GO analyses of upregulated (C) and downregulated (D) differentially expressed genes.

PKA $\alpha$ R allele) that coexpresses ACTA2 is expanded. Interestingly, it was recently reported that *H. pylori* infection in the mouse stomach leads to expansion of ACTA2<sup>+</sup>/MYH11<sup>+</sup> stromal population that expressed high levels of BMP antagonists including gremlin 1.<sup>11</sup> These results strongly suggest that the *H. pylori*-targeted stromal cells that include the ACTA2<sup>+</sup> stromal population responsible for secreting BMP antagonists, including gremlin 1, is expanded in CA-PKA mice. Together, these results set a foundation for further studies to determine whether aberrant PKA activation occurs and contributes towards the pathogenesis of *H. pylori*-induced gastritis.

We determined the molecular signature of the PKA $\alpha$ R-induced inflammatory program and identified STAT3 activation in both epithelial and stromal compartments that was possibly driven by increased IL11 and IL1a. In addition to gastric preneoplasia and adenocarcinoma, aberrant STAT3 activation and induction of a similar inflammatory program also occurs in PJS, caused by inactivating LKB1 mutations.<sup>48,50,51</sup> Patients with PJS develop gastric polyps and are at a high risk of developing tumors in the stomach and other organs. It was recently demonstrated that stromal cells lacking LKB1 activity displayed dramatic upregulation and secretion of inflammatory cytokines including IL11,

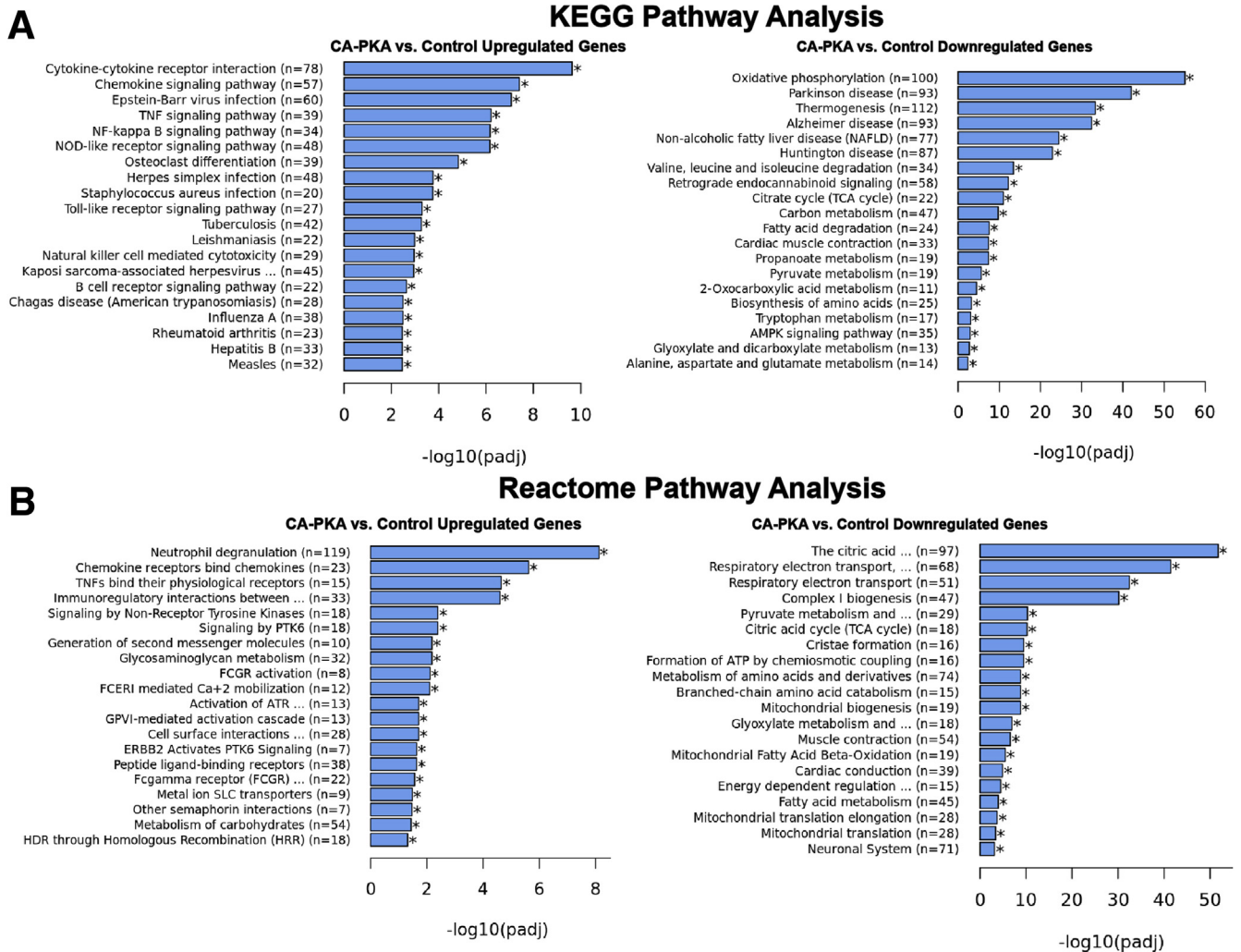


**Figure 10.** Kyoto Encyclopedia of Genes and Genomes and Reactome pathway analysis of control and CA-PKA corpus identify misregulation of pathways involved in immune response and metabolism (A–B). A, Top 20 pathways revealed by separate Kyoto Encyclopedia of Genes and Genomes analyses of upregulated and downregulated differentially expressed genes. B, Top 20 pathways revealed by separate Reactome analyses of upregulated and downregulated differentially expressed genes.

indicating a causative role of stromal population in inciting the inflammatory microenvironment.<sup>48</sup> Determining whether inappropriate activation of PKA in stromal cells initiates secretion of inflammatory cytokines that precedes and contributes to inflammatory cell infiltration and parietal cell loss will be important to establish a causative role of PKA in initiating inflammation.

The CA-PKA mouse model recapitulates nearly the full spectrum of classic metaplastic and preneoplastic lesions in the stomach. We observed changes in the expression levels of multiple canonical SPEM transcripts that were similar to those known to be altered in human gastric preneoplastic lesions and models of gastric preneoplasia in which SPEM cells are developed either by drug-induced acute parietal cell loss or chronic inflammation.<sup>41</sup> Intestinal metaplasia is one of the key preneoplastic lesions observed in human intestinal-type gastric adenocarcinoma and is characterized by the presence of AB-stained goblet cells.<sup>33,44,64</sup> Corpus

mucosa of CA-PKA mice displayed dramatic upregulation of various transcripts associated with metaplasia, a dramatic switch in secreting acid mucins and also showed expression of MUC2, a well-established marker of intestinal metaplasia. In the antrum of CA-PKA mice with severe lesions, we did observe AB-stained goblet cells and expression of MUC2 that are classic features of intestinal metaplasia observed in only a few models of gastric preneoplasia.<sup>33,65-67</sup> Another key attribute of the CA-PKA model was dysplastic glands that frequently invaded very deep into the submucosa and even into the mucosa with sharp increases in associated matrix metalloprotease expression that likely facilitated the invasion.<sup>65</sup>

Signaling pathways including BMP, ERK, sonic hedgehog, fibroblast growth factor, and Wnt are known to regulate stomach patterning and homeostasis and contribute to MEC.<sup>3,68,69</sup> Our study identifies PKA signaling as a novel player in gastric MEC execution by regulating BMP and ERK

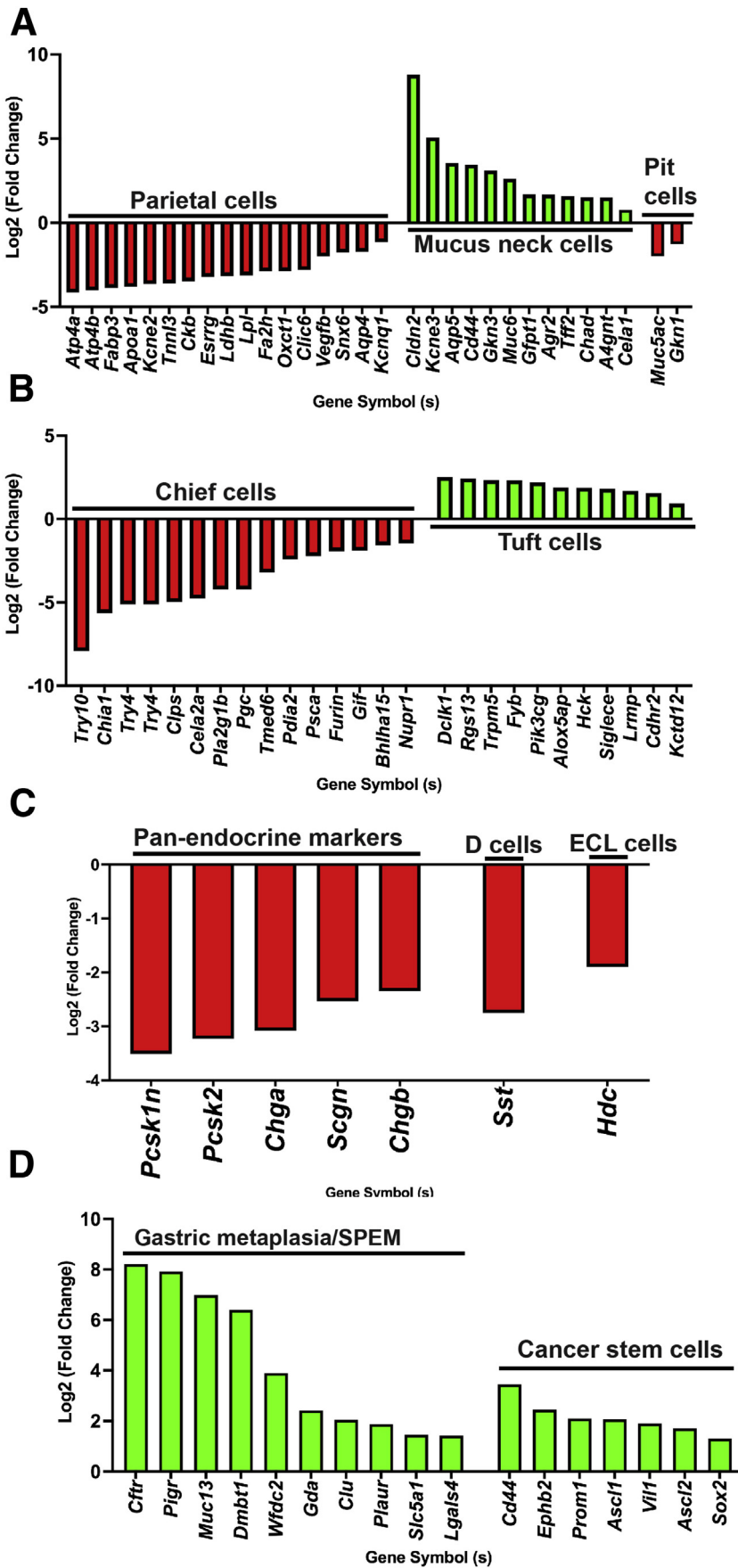


**Figure 11.** mRNA seq analysis identify misregulated gene expression indicating cellular alterations in CA-PKA stomach (A-D). Fold change in differentially expressed genes enriched in parietal cell, mucous neck and pit cells (A); chief cells and tuft cells (B); endocrine cells (C); and in the markers of gastric metaplasia and cancer stem cells (D). All data with green and red bars show significant gene changes with P value of .05 or less.



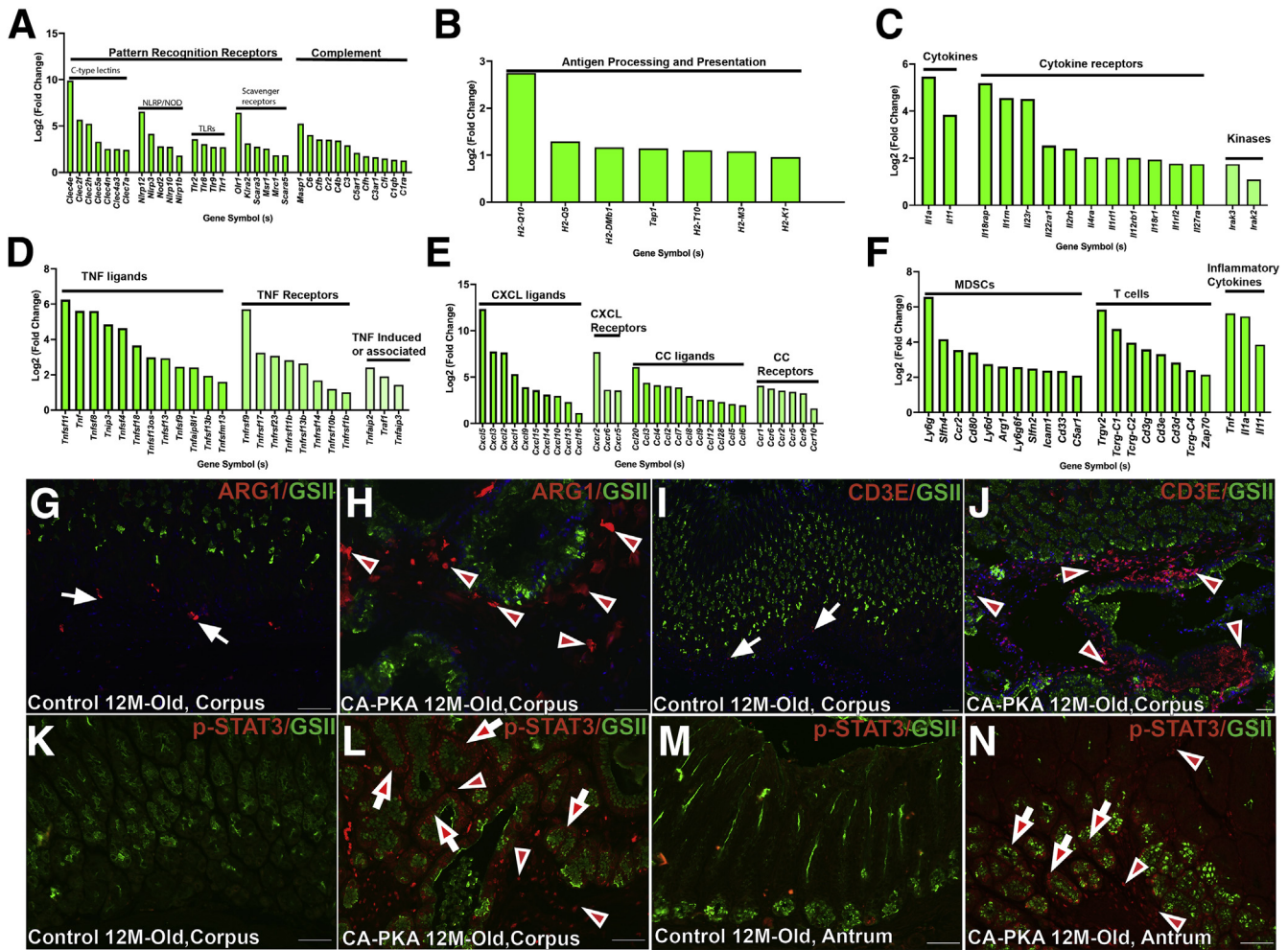


**Figure 12.** mRNA seq identifies multiple molecular and cellular components of potent inflammatory microenvironment in CA-PKA corpus stomach (A–F). RNA seq analysis of CA-PKA mice vs control corpus stomach (fold-change) for components of innate immune system (A), genes involved in antigen processing and presentation that are an important component of adaptive immune system (B), interleukins, interleukin receptors, and associated kinases (C), TNF ligands, receptors, and TNF-induced proteins receptors (D), chemokines of CXCL and CCL categories and their receptors (E), and in the markers of myeloid-derived suppressor cells, T lymphocytes, and inflammatory cytokines (F). All data with green bars show significant gene changes with *P* value of .05 or less. G–J, Corpus sections of 12-month-old control and CA-PKA mice co-stained with GSII-lectin (green) and either ARG1 (red, myeloid-derived suppressor cells) or CD3ε (red, T cells) antisera. In control (G & I), ARG1 (arrows) and CD3ε (arrows) were rarely detected; in mutant, ARG1<sup>+</sup> (H) (arrowheads) and CD3ε<sup>+</sup> cells (J) (arrowheads) were increased. K–N, Corpus and antrum sections of control and CA-PKA mice co-stained with phospho-STAT3 antiserum (red) and GSII-lectin (green). In control corpus (K) and antrum (M), p-STAT3 signal was undetectable; in mutant, p-STAT3 was detected in epithelial (arrows) and stromal cells (arrowheads) of both corpus (L) and antrum (N). Scale bars = 50 μm.

pathways. We found that disruption of gastric homeostasis by mesenchymal PKA $\alpha$ R is at least partly driven by BMP signaling inhibition. Previously, inhibition of BMP signaling by parietal cell-specific expression of BMP inhibitor, noggin, led to decreased parietal cell number, likely by impairing differentiation.<sup>5</sup> It is possible that in CA-PKA mutants, PKA-mediated inhibition of BMP signaling impairs parietal cell differentiation contributing to their depletion. Inhibition or loss of BMP signaling in the stomach epithelial and mesenchymal compartments caused inflammation, epithelial hyperproliferation, and dysplasia; these similar aberrations were observed in CA-PKA mutants.<sup>4,6</sup> Furthermore, germline mutations in BMP signaling components *Bmpr1a* and

*Smad4* lead to the development of PJS, which causes hamartoma's polyps characterized by marked inflammation and cystic glands and predisposition for gastrointestinal cancers including stomach.<sup>70-72</sup> Although our studies show that the development of inflammation and preneoplastic state in CA-PKA mice are associated with the downregulation of BMP signaling, further studies will be required to establish a causative role of downregulated BMP signaling in the gastric pathology observed in CA-PKA mice.

Multiple BMP signaling components were significantly altered in CA-PKA mutants, including a dramatic upregulation of BMP antagonist, gremlin 1. Notably, gremlin 1 upregulation in intestinal fibroblasts was recently shown to

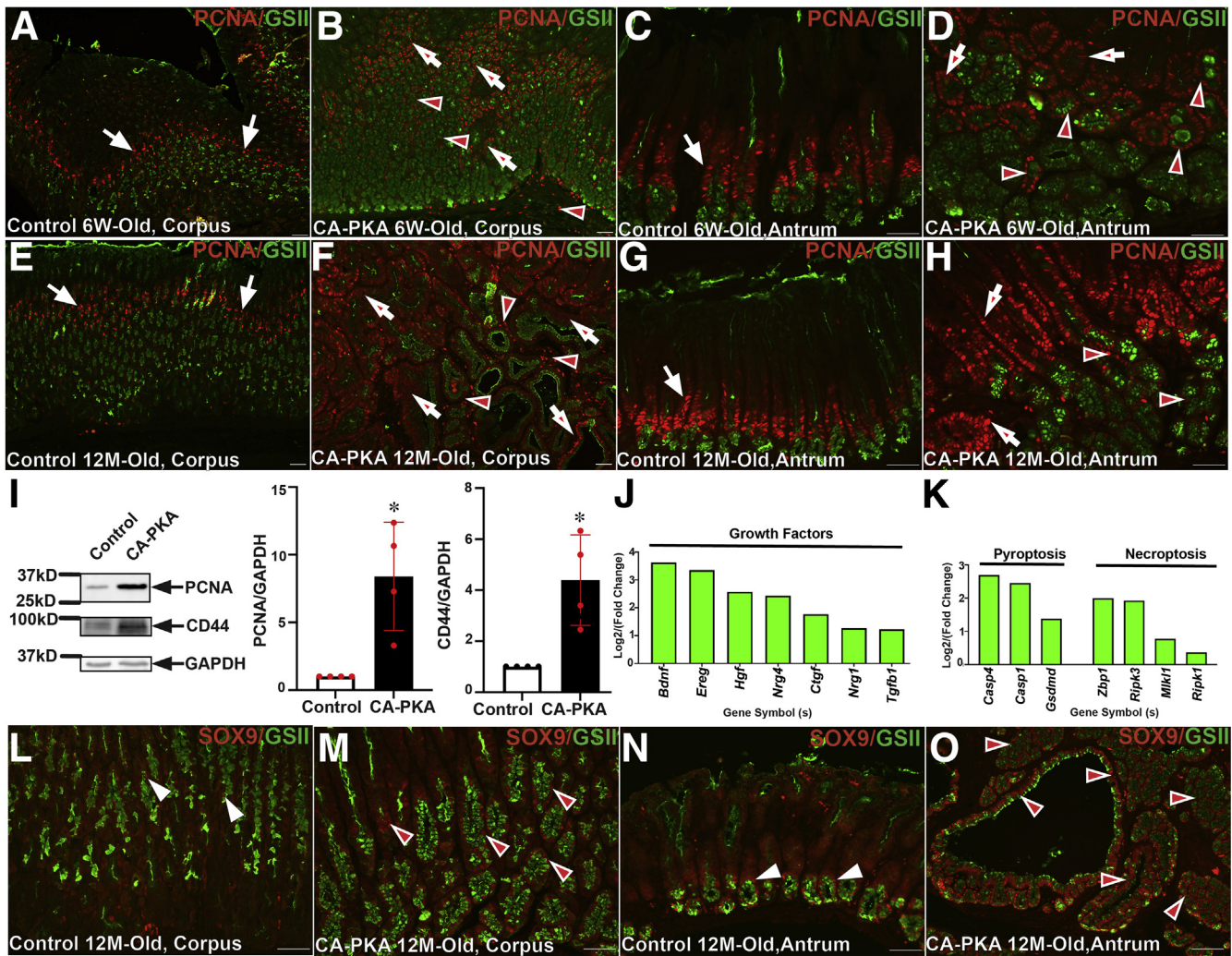


**Figure 13. Increased proliferation and dedifferentiation markers in CA-PKA mice.** A–H, Stomach sections from 6-week- and 12-month-old control and CA-PKA mice co-stained with PCNA antiserum (red, proliferation) and GSII-lectin (green). Arrows show proliferation zone in control corpus (A & E) and antrum (C & G). In 6-week- and 12-month-old mutant corpus (B & F), increased PCNA<sup>+</sup> cells are shown in the epithelial (arrows) and stromal (arrowheads) compartments; and in the neck (arrows) and base (arrowheads) of the mutant antral glands (D & H). I, Representative immunoblots and quantification graphs (\**P* < .05) showing relative PCNA (n = 4) and CD44 (n = 4) levels in the corpus of CA-PKA mutants vs control. Fold change (*P* < .05 or less) in the markers of (J) growth factors and genes involved in (K) pyroptosis and necroptosis identified by RNAseq. All data with green bars show significant gene changes with *P* value of .05 or less. L–O. Corpus and antrum sections of 12-month-old control and CA-PKA mice co-stained with SOX9 antiserum (red, dedifferentiation) and GSII-lectin (green). In control corpus (L), SOX9 is shown in a few epithelial cells (arrowheads); and in the base of antral glands (arrowheads) (N). SOX9<sup>+</sup> cells were dramatically increased in the mutant corpus (arrowheads) (M); and antrum (arrowheads) (O). Scale bars = 50  $\mu$ m.

inhibit BMP signaling and drive dedifferentiation in the intestinal mucosa following injury.<sup>53</sup> Because dedifferentiation markers including CD44 and SOX9 were upregulated in association with increased cell proliferation, it will be important to determine the extent by which the observed gastric pathology in CA-PKA mutants is due to PKA-mediated inhibition of BMP signaling and gremlin 1 upregulation.

We also observed activation of ERK1/2 localized in the mesenchymal compartment. Aberrant ERK activation in gastric stromal fibroblasts is known to support proliferation of cancer cells by constituting a tumor cell niche.<sup>13</sup> cAMP/PKA signaling crosstalks with ERK1/2 signaling to stimulate

proliferation.<sup>16,17</sup> ERK1/2 activation that occurs in CA-PKA mice likely contributes to the proliferation of mesenchymal population. Given that multiple cytokines and chemokines activate ERK signaling that further stimulates inflammation, another possible source of activated ERK1/2 is highly increased levels of cytokines and chemokines in the CA-PKA mouse stomach.<sup>73–75</sup> Further studies will be required to dissect a causative role of aberrantly activated ERK signaling in hyperproliferation and/or inflammation in CA-PKA mice.

PKA is a well-known transducer of beta-2 adrenergic signaling.<sup>76</sup> In vitro studies have shown that beta-2 adrenergic signaling not only contributes to chronic stress-

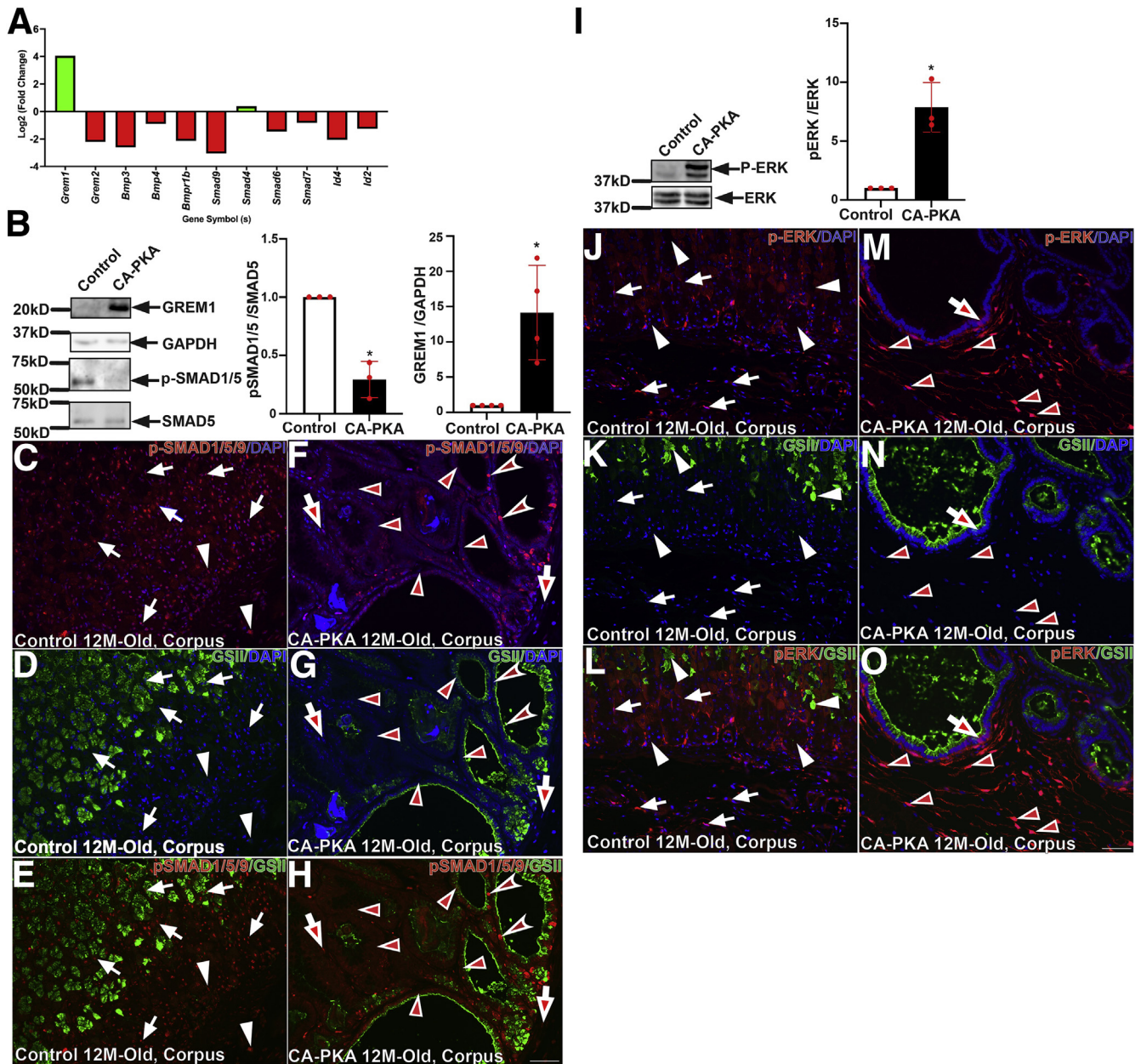
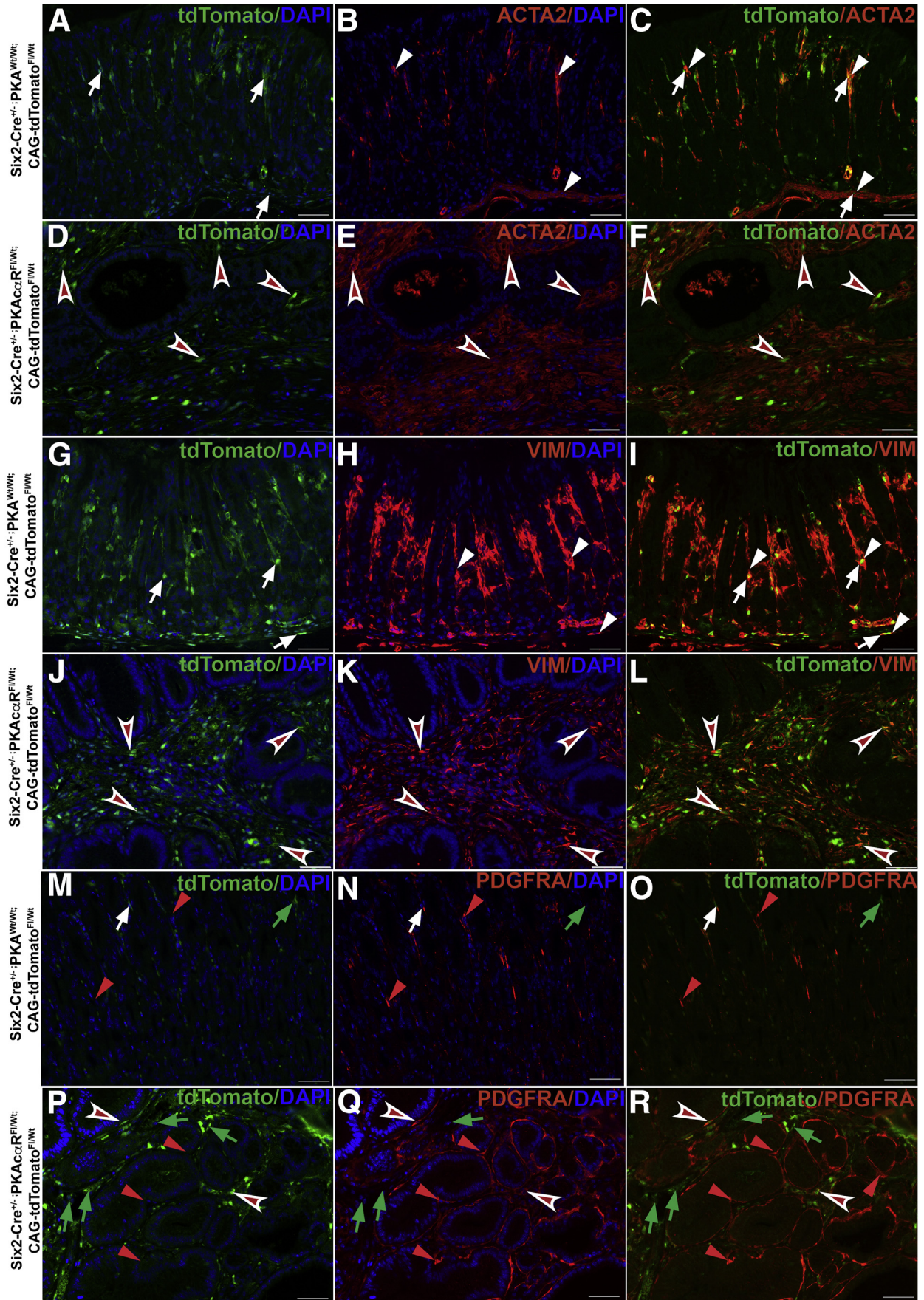


**Figure 14. BMP and ERK signaling is misregulated in CA-PKA corpus.** *A*, Fold change ( $P < .05$  or less) in BMP pathway components identified by RNAseq. *B*, Representative immunoblots and quantification graphs ( $*P < .05$ ) showing relative gremlin 1 (GREM1) and phospho-SMAD1/5 levels in the mutant corpus vs control. *C–H*, Corpus sections from 12-month-old control and CA-PKA mice co-stained with phospho-SMAD1/5/9 antiserum (red, BMP response) and GSII-lectin (green). In control corpus (*C* & *E*), phospho-SMAD1/5/9 signal was observed in epithelial (arrows) and stromal (arrowheads) compartments. In the mutant corpus (*F* & *H*), decreased phospho-SMAD1/5/9 signal is indicated in epithelial (arrowheads) and stromal (arrows) compartments; a few epithelial (concave arrowheads) with strong phospho-SMAD1/5/9 signal are indicated. *I*, Representative immunoblot and quantification graph ( $*P < .05$ ) showing phospho-ERK ( $n = 4$ ) levels in the corpus of CA-PKA mutants vs control. *J–O*, Images of corpus sections of 12-month-old control and CA-PKA mice co-stained with p-ERK1/2 antiserum (red) and GSII-lectin (green). In control corpus (*J–L*), cytoplasmic p-ERK signal in parietal (white arrows) and stromal cells (white arrowheads) is indicated. In mutant corpus (*M–O*), nuclear p-ERK signal in stromal cells (arrowheads) and cytoplasmic p-ERK signal in an epithelial cell (arrow) is shown. Scale bars = 50  $\mu\text{m}$ . Blue (DAPI).

induced gastric cancer progression and metastasis, but also mediates desensitization of gastric cancer cells to targeted chemotherapies.<sup>77,78</sup> These effects of adrenergic signaling on gastric cancer cells were found to be mediated by ERK and STAT3 signaling as well as the CREB transcription

factor.<sup>77,78</sup> Our CA-PKA mice also show activation of ERK, STAT3 and CREB. It will be important to determine whether PKA signaling in the stomach mesenchyme acts as a modifier and exacerbates dysplasia into adenocarcinomas in preclinical gastric cancer models.



In this study, we characterized the activity of Cre-recombinase driven by the Six2-Cre promoter in the stomach by lineage tracing. Six2-Cre transgenic mouse line has been extensively used to induce recombination in the mesenchymal nephron progenitors of the kidney.<sup>24,29,79</sup> Six2-Cre activity also was reported previously in the stomach, but, not fully characterized.<sup>31,80</sup> In addition to kidney and stomach, Six2-cre activity was also reported in the developing head, ear, limb, and osteoprogenitor cells.<sup>24,81</sup> Six2-Cre-mediated recombination has not been observed in the thymus, brain, lung, intestine, liver, spleen, and myeloid cells.<sup>80,82</sup> Based on the extensive cellular and molecular phenotyping of CA-PKA mice, along with the characterization of Six2-Cre activity performed, and the information available about Six2-Cre activity in the literature, all aspects of the gastric pathology observed in CA-PKA mice are likely to be due to PKA activation in the gastric mesenchyme. Notably, genetic modifications of LKB1 signaling in T lymphocytes has been reported to be sufficient to derive inflammation and polyposis in the gut.<sup>83</sup> Therefore, to definitively rule out any gastric-extrinsic contribution of PKA activation in the pathology of CA-PKA mice, generation and phenotyping of additional cell-specific conditional mutants will be required.

In summary, our findings identify a novel role of PKA signaling in the execution of gastric MEC and show that PKA activation in the gastric mesenchyme disrupts gastric homeostasis and drives preneoplastic state that is associated with the downregulation of BMP signaling activation of ERK1/2. Our findings showing that gastric mesenchymal PKA activation can drive a proliferative and proinflammatory microenvironment, suggesting that the misregulation of PKA signaling is a potential contributor to various inflammation-based gastric pathologies such as gastritis, polyposis, and cancer.<sup>47,48,64</sup>

## Methods

### Mice

Mice harboring constitutively active mutation in the *Prkca* encoding PKA $\alpha$  were rederived from the Mutant Mouse Regional Resource Centers at the University of Missouri (032825-MU) on a C57BL/6Ncrl

background and maintained by breeding with C57BL/6J mice. *Tg(Six2-EGFP/cre)1Amc* (herein *Six2-Cre*) (strain #009606) rederived from the Jackson laboratory were on CD1 background. Mutant CA-PKA (double heterozygous with mixed background) mice were obtained by mating *Six2cre*<sup>+/-</sup> mice with mice carrying 1 floxed *Prkca* mutant allele and genotyped as previously described.<sup>23,24</sup> For all experiments shown, *Six2cre*<sup>+/-</sup> PKA $\alpha$ R<sup>wt/wt</sup> littermates were used as controls, but if not available, *Six2cre*<sup>-/-</sup> PKA $\alpha$ R<sup>fl/wt</sup> littermates were used as controls. At least 3 male and female mice were used for 6-week-old and 8- to 12-month-old time points, and no sex-based differences were found in phenotype penetrance and severity. For lineage tracing studies, *Six2cre*<sup>+/-</sup> transgenic mice were bred with Ai9 (RCL-*tdTomato*) mice (Stock # 007909), (129S6/SvEvTac x C57BL/6Ncrl) to generate *Six2cre*<sup>+/-</sup>;*CAG-tdTomato*<sup>+/-</sup>. To generate *Six2-Cre*<sup>+/-</sup>-PKA $\alpha$ R<sup>fl/wt</sup>;R-*tdTomato*<sup>fl/wt</sup> mice, PKA $\alpha$ R<sup>fl/wt</sup> mice were bred with *Six2cre*<sup>+/-</sup>;*CAG-tdTomato*<sup>+/-</sup> mice. Animals used in these studies were maintained and euthanized according to the principles and procedures described in the National Institutes of Health Guide for the Care and Use of Laboratory Animals. These studies were approved by the Tuskegee University Institutional Animal Care and Use Committee.

### Histology and Co-IF Microscopy

For histological studies, 4  $\mu$ m paraformaldehyde-fixed paraffin embedded stomach sections were deparaffinized, rehydrated, and subjected to hematoxylin and eosin staining. For AB staining, sections were stained for 30 minutes in 1% AB in 3% acetic acid pH 2.5, washed and counterstained with 0.1% nuclear fast red solution for 5 minutes and then washed, dehydrated, and mounted. For PAS/AB staining, sections stained with AB were oxidized in 0.5% PAS for 15 minutes, washed and placed in Schiff reagent for 30 minutes followed by rinsing, counterstaining with hematoxylin and were dehydrated and mounted. For co-IF studies, rehydrated sections were subjected to antigen retrieval in citrate buffer (10 mM citrate, 0.1% Tween-20, pH 9.0) at 95 °C for 30 minutes and then kept at room temperature for 30 minutes. The sections were blocked for 1 hour in donkey serum at room

**Figure 15. (See previous page). Characterization of stromal cell alterations in Six2-Cre<sup>+/-</sup>-PKA $\alpha$ R<sup>fl/wt</sup>;R-tdTomato<sup>fl/wt</sup> corpus.** A–F, Corpus sections from 8M-old Six2-Cre<sup>+/-</sup>;PKA<sup>wt/wt</sup>; R-tdTomato<sup>fl/wt</sup> (control) and Six2-Cre<sup>+/-</sup>-PKA $\alpha$ R<sup>fl/wt</sup>;R-tdTomato<sup>fl/wt</sup> (mutant) mice co-stained with RFP (green) (staining tdTomato) and ACTA2 antisera (red). In control (A–C), RFP (arrows) and ACTA2 (arrowheads) double-positive stromal cells present underneath, in between gastric glands and in the muscularis mucosae are indicated. In mutant (D–F), RFP/ACTA2 double-positive cell population is markedly expanded (arrowheads) and is present underneath and in between invading and cystic glands. G–L, Corpus sections from 8M-old Six2-Cre<sup>+/-</sup>;PKA<sup>wt/wt</sup>; R-tdTomato<sup>fl/wt</sup> (control) and Six2-Cre<sup>+/-</sup>-PKA $\alpha$ R<sup>fl/wt</sup>;R-tdTomato<sup>fl/wt</sup> (mutant) mice co-stained with RFP (green) (staining tdTomato) and VIM antisera (red). In control (G–I), RFP (arrows) and VIM (arrowheads) double-positive stromal cells present underneath, in between gastric glands and in the muscularis mucosae are indicated. In mutant (J–L), RFP/VIM double-positive cell population is markedly expanded (arrowheads) and is present underneath and in between invading and cystic glands. M–R, Corpus sections from 8M-old Six2-Cre<sup>+/-</sup>;PKA<sup>wt/wt</sup>; R-tdTomato<sup>fl/wt</sup> (control) and Six2-Cre<sup>+/-</sup>-PKA $\alpha$ R<sup>fl/wt</sup>;R-tdTomato<sup>fl/wt</sup> (mutant) mice co-stained with RFP (green) (staining tdTomato) and PDGFRA antisera (red). In control (M–O), RFP<sup>+</sup>/PDGFRA<sup>-</sup> (green arrows), RFP<sup>+</sup>/PDGFRA<sup>+</sup> (red arrowheads), and RFP<sup>+</sup>/PDGFRA<sup>+</sup> (white arrows) cells present in between gastric glands are indicated. In mutant (P–R), RFP<sup>+</sup>/PDGFRA<sup>+</sup> (red arrowheads) expanded cell population localized around the glands is indicated. RFP<sup>+</sup>/PDGFRA<sup>-</sup> (green arrows), was expanded present in between cystic glands is indicated. Relatively fewer RFP<sup>+</sup>/PDGFRA<sup>+</sup> (concave arrowheads) cells are indicated. Scale bars = 50  $\mu$ m. Blue (DAPI).

temperature and incubated for 12 to 18 hours with primary antibodies or lectins with dilutions mentioned in [Supplementary Table 1](#), followed by washing and 1 hour incubation with appropriate secondary antibodies. Images were captured using Olympus fluorescence BX53F microscope (Leica, Wetzlar, Germany).

### Immunoblotting

For preparing whole cell lysates, corpus tissue without contamination from forestomach or antrum was isolated from 8- to 12-month-old control and mutant mice and homogenized in RIPA lysis buffer (AAJ62524AE, Alfa Aesar) supplemented with a protease inhibitor cocktail (Cat # 78425, Thermo Fisher). The solution was sonicated 6 times for 3 seconds and rocked for 30 minutes at 4 °C to extract proteins followed by centrifugation at 14,000 × g for 30 minutes. Protein quantification was performed by Pierce BCA Protein Assay Kit (Cat#23225) Supernatant mixed with Laemmli buffer was used for immunoblotting. Cell lysates were separated by SDS-PAGE, transferred to nitrocellulose membranes, and blocked with 5% non-fat dry milk in TBST (blocking buffer) and incubated with primary antibodies in blocking buffer with dilutions detailed in [Supplementary Table 1](#). Following washing in TBST, membranes were incubated with secondary antibody conjugated with horseradish peroxidase diluted at 1:1000. The protein-antibody complex was visualized with supersignal west dura extended duration substrate (Pierce) in Amersham Imager 680 RGB system.

### mRNA Sequencing and Bioinformatics Analysis

Corpus samples isolated from 7- to 8-month-old control ( $n = 4$ ) and mutant ( $n = 4$ ) mice were sent to Novogene Bioinformatics Technology Co, Ltd, in Beijing, China for RNA extraction and mRNA sequencing. Total RNA was isolated using the TRIzol reagent, and RNA quality was assessed on nanodrop and agarose electrophoresis. RNA integrity and quantification were assessed using the RNA Nano 6000 assay kit of the Bioanalyzer 2100 system (Agilent Technologies). A total amount of 1 µg RNA per sample was used as input material for the RNA sample preparations. Sequencing libraries were generated using NEBNext Ultra RNA Library Prep Kit for Illumina (NEB) following manufacturer's recommendations, and index codes were added to attribute sequences to each sample. The clustering of the index-coded samples was performed on a cBot Cluster Generation System using PE Cluster Kit cBot-HS (Illumina) according to the manufacturer's instructions. After cluster generation, preparations were sequenced on an Illumina platform and paired-end reads were generated. Raw data of FASTQ format were first processed through fastp. In this step, clean data (clean reads) were obtained by removing reads containing adapter sequences and reads with low quality. All the downstream analyses were based on clean data with high quality. Reference genome and gene model annotation files were downloaded from genome website browser

(NCBI/UCSC/Ensembl) directly. Indexes of the reference genome were built using STAR, and paired-end clean reads were aligned to the reference genome using STAR (v2.5). FeatureCounts was used to count the read numbers mapped of each gene, and then FPKM of each gene was calculated based on the length of the gene and reads count mapped to this gene. All raw and processed mRNA seq data has been submitted to GEO repository (#GSE196236).

### Bioinformatics and Statistical Analysis

Differential expression analysis between 2 conditions/groups was performed using the DESeq2 R package (2.1.6.3). The resulting *P*-values were adjusted using the Benjamini and Hochberg's approach for controlling the false discovery rate (FDR). Genes with an adjusted *P*-value < .05 found by DESeq2 were assigned as differentially expressed. GO enrichment analysis of differentially expressed genes was implemented by the clusterProfiler R package, in which gene length bias was corrected. GO terms with corrected *P*-value less than .05 were considered significantly enriched by differential expressed genes. We used clusterProfiler R package to test the statistical enrichment of differential expression genes in Kyoto Encyclopedia of Genes and Genomes and REACTOME pathways. Immunoreactive signals from Western blot films were quantified using National Institutes of Health image J software, and results were analyzed by t test using GraphPad Prism software (GraphPad Software, LA Jolla, CA).

### References

1. Le Guen L, Marchal S, Faure S, de Santa Barbara P. Mesenchymal-epithelial interactions during digestive tract development and epithelial stem cell regeneration. *Cell Mol Life Sci* 2015;72:3883–3896.
2. Zhang Y, Que J. BMP signaling in development, stem cells, and diseases of the gastrointestinal tract. *Annu Rev Physiol* 2020;82:251–273.
3. Kim TH, Shivdasani RA. Stomach development, stem cells and disease. *Development* 2016;143:554–565.
4. Roy SAB, Allaire JM, Ouellet C, Maloum-Rami F, Pomerleau V, Lemieux E, Babeu JP, Rousseau J, Paquet M, Garde-Granger P, Boudreau F, Perreault N. Loss of mesenchymal bone morphogenetic protein signaling leads to development of reactive stroma and initiation of the gastric neoplastic cascade. *Sci Rep* 2016;6:32759.
5. Shinohara M, Mao M, Keeley TM, El-Zaatari M, Lee HJ, Eaton KA, Samuelson LC, Merchant JL, Goldenring JR, Todisco A. Bone morphogenetic protein signaling regulates gastric epithelial cell development and proliferation in mice. *Gastroenterology* 2010;139:2050–2060.e2.
6. Todisco A. Regulation of gastric metaplasia, dysplasia, and neoplasia by bone morphogenetic protein signaling. *Cell Mol Gastroenterol Hepatol* 2017;3:339–347.
7. Takabayashi H, Shinohara M, Mao M, Phaosawadi P, El-Zaatari M, Zhang M, Ji T, Eaton KA, Dang D, Kao J, Todisco A. Anti-inflammatory activity of bone

- morphogenetic protein signaling pathways in stomachs of mice. *Gastroenterology* 2014;147:396–406.e7.
8. Correa P. Human gastric carcinogenesis: a multistep and multifactorial process—First American Cancer Society Award Lecture on Cancer Epidemiology and Prevention. *Cancer Res* 1992;52:6735–6740.
  9. Uemura N, Okamoto S, Yamamoto S, Matsumura N, Yamaguchi S, Yamakido M, Taniyama K, Sasaki N, Schlemper RJ. *Helicobacter pylori* infection and the development of gastric cancer. *N Engl J Med* 2001; 345:784–789.
  10. Houghton J, Wang TC. *Helicobacter pylori* and gastric cancer: a new paradigm for inflammation-associated epithelial cancers. *Gastroenterology* 2005; 128:1567–1578.
  11. Kapalczynska M, Lin M, Maertzdorf J, Heuberger J, Muellerke S, Zuo X, Vidal R, Shureiqi I, Fischer AS, Sauer S, Berger H, Kidess E, Mollenkopf HJ, Tacke F, Meyer TF, Sigal M. BMP feed-forward loop promotes terminal differentiation in gastric glands and is interrupted by *H. pylori*-driven inflammation. *Nat Commun* 2022;13:1577.
  12. Sigal M, Rothenberg ME, Logan CY, Lee JY, Honaker RW, Cooper RL, Passarelli B, Camorlinga M, Bouley DM, Alvarez G, Nusse R, Torres J, Amieva MR. *Helicobacter pylori* activates and expands Lgr5(+) stem cells through direct colonization of the gastric glands. *Gastroenterology* 2015;148:1392–1404.e21.
  13. Kikuchi Y, Kunita A, Iwata C, Komura D, Nishiyama T, Shimazu K, Takeshita K, Shibahara J, Kii I, Morishita Y, Yashiro M, Hirakawa K, Miyazono K, Kudo A, Fukayama M, Kashima TG. The niche component periostin is produced by cancer-associated fibroblasts, supporting growth of gastric cancer through ERK activation. *Am J Pathol* 2014;184:859–870.
  14. Gupta IR, Piscione TD, Grisaru S, Phan T, Macias-Silva M, Zhou X, Whiteside C, Wrana JL, Rosenblum ND. Protein kinase A is a negative regulator of renal branching morphogenesis and modulates inhibitory and stimulatory bone morphogenetic proteins. *J Biol Chem* 1999;274:26305–26314.
  15. Puri P, Little-Ihrig L, Chandran U, Law NC, Hunzicker-Dunn M, Zeleznik AJ. Protein Kinase A: a master kinase of granulosa cell differentiation. *Sci Rep* 2016;6:28132.
  16. Stork PJ, Schmitt JM. Crosstalk between cAMP and MAP kinase signaling in the regulation of cell proliferation. *Trends Cell Biol* 2002;12:258–266.
  17. Yamaguchi T, Nagao S, Wallace DP, Belibi FA, Cowley BD, Pelling JC, Grantham JJ. Cyclic AMP activates B-Raf and ERK in cyst epithelial cells from autosomal-dominant polycystic kidneys. *Kidney Int* 2003;63:1983–1994.
  18. Kirschner LS, Carney JA, Pack SD, Taymans SE, Giatzakis C, Cho YS, Cho-Chung YS, Stratakis CA. Mutations of the gene encoding the protein kinase A type I- $\alpha$  regulatory subunit in patients with the Carney complex. *Nat Genet* 2000;26:89–92.
  19. Molyneux SD, Di Grappa MA, Beristain AG, McKee TD, Wai DH, Paderova J, Kashyap M, Hu P, Maiuri T, Narala SR, Stambolic V, Squire J, Penninger J, Sanchez O, Triche TJ, Wood GA, Kirschner LS, Khokha R. Prkar1a is an osteosarcoma tumor suppressor that defines a molecular subclass in mice. *J Clin Invest* 2010;120:3310–3325.
  20. Beristain AG, Molyneux SD, Joshi PA, Pomroy NC, Di Grappa MA, Chang MC, Kirschner LS, Prive GG, Pujana MA, Khokha R. PKA signaling drives mammary tumorigenesis through Src. *Oncogene* 2015; 34:1160–1173.
  21. Sahoo N, Gu M, Zhang X, Raval N, Yang J, Bekier M, Calvo R, Patnaik S, Wang W, King G, Samie M, Gao Q, Sahoo S, Sundaresan S, Keeley TM, Wang Y, Marugan J, Ferrer M, Samuelson LC, Merchant JL, Xu H. Gastric acid secretion from parietal cells is mediated by a Ca(2+) efflux channel in the tubulovesicle. *Dev Cell* 2017; 41:262–273.e6.
  22. Kirschner LS, Yin Z, Jones GN, Mahoney E. Mouse models of altered protein kinase A signaling. *Endocr Relat Cancer* 2009;16:773–793.
  23. Niswender CM, Willis BS, Wallen A, Sweet IR, Jetton TL, Thompson BR, Wu C, Lange AJ, McKnight GS. Cre recombinase-dependent expression of a constitutively active mutant allele of the catalytic subunit of protein kinase A. *Genesis* 2005;43:109–119.
  24. Kobayashi A, Valerius MT, Mugford JW, Carroll TJ, Self M, Oliver G, McMahon AP. Six2 defines and regulates a multipotent self-renewing nephron progenitor population throughout mammalian kidney development. *Cell Stem Cell* 2008;3:169–181.
  25. Tascou L, Gardner T, Anan H, Yongpravat C, Cardozo CP, Bauman WA, Lee FY, Oh DS, Tawfeek HA. Activation of protein kinase A in mature osteoblasts promotes a major bone anabolic response. *Endocrinology* 2016;157:112–126.
  26. Ognjenovic NB, Bagheri M, Mohamed GA, Xu K, Chen Y, Mohamed Saleem MA, Brown MS, Nagaraj SH, Muller KE, Gerber SA, Christensen BC, Pattabiraman DR. Limiting self-renewal of the basal compartment by PKA activation induces differentiation and alters the evolution of mammary tumors. *Dev Cell* 2020;55(5):544–557.e6.
  27. Kao RS, Abbott MJ, Louie A, O'Carroll D, Lu W, Nissenson R. Constitutive protein kinase A activity in osteocytes and late osteoblasts produces an anabolic effect on bone. *Bone* 2013;55:277–287.
  28. Lin RZ, Chen J, Hu ZW, Hoffman BB. Phosphorylation of the cAMP response element-binding protein and activation of transcription by alpha1 adrenergic receptors. *J Biol Chem* 1998;273:30033–30038.
  29. Puri P, Schaefer CM, Bushnell D, Taglienti ME, Kreidberg JA, Yoder BK, Bates CM. Ectopic phosphorylated Creb marks dedifferentiated proximal tubules in cystic kidney disease. *Am J Pathol* 2018;188:84–94.
  30. Oliver G, Wehr R, Jenkins NA, Copeland NG, Cheyette BN, Hartenstein V, Zipursky SL, Gruss P. Homeobox genes and connective tissue patterning. *Development* 1995;121:693–705.
  31. Kiefer SM, Robbins L, Rauchman M. Conditional expression of Wnt9b in Six2-positive cells disrupts stomach and kidney function. *PLoS One* 2012;7:e43098.

32. Burkitt MD, Varro A, Pritchard DM. Importance of gastrin in the pathogenesis and treatment of gastric tumors. *World J Gastroenterol* 2009;15:1–16.
33. Petersen CP, Mills JC, Goldenring JR. Murine models of gastric corpus preneoplasia. *Cell Mol Gastroenterol Hepatol* 2017;3:11–26.
34. Rieder G, Tessier AJ, Qiao XT, Madison B, Gumucio DL, Merchant JL. Helicobacter-induced intestinal metaplasia in the stomach correlates with Elk-1 and serum response factor induction of villin. *J Biol Chem* 2005;280:4906–4912.
35. Hagen SJ, Ang LH, Zheng Y, Karahan SN, Wu J, Wang YE, Caron TJ, Gad AP, Muthupalani S, Fox JG. Loss of tight junction protein claudin 18 promotes progressive neoplasia development in mouse stomach. *Gastroenterology* 2018;155:1852–1867.
36. Fristedt R, Gaber A, Hedner C, Nodin B, Uhlen M, Eberhard J, Jirstrom K. Expression and prognostic significance of the polymeric immunoglobulin receptor in esophageal and gastric adenocarcinoma. *J Transl Med* 2014;12:83.
37. Buslinger GA, Weusten BLA, Bogte A, Begthel H, Brosens LAA, Clevers H. Human gastrointestinal epithelia of the esophagus, stomach, and duodenum resolved at single-cell resolution. *Cell Rep* 2021;34:108819.
38. Mills JC, Syder AJ, Hong CV, Guruge JL, Raaii F, Gordon JI. A molecular profile of the mouse gastric parietal cell with and without exposure to *Helicobacter pylori*. *Proc Natl Acad Sci U S A* 2001;98:13687–13692.
39. Lambrecht NW, Yakubov I, Zer C, Sachs G. Transcriptomes of purified gastric ECL and parietal cells: identification of a novel pathway regulating acid secretion. *Physiol Genomics* 2006;25:153–165.
40. Lee HJ, Nam KT, Park HS, Kim MA, Laflour BJ, Aburatani H, Yang HK, Kim WH, Goldenring JR. Gene expression profiling of metaplastic lineages identifies CDH17 as a prognostic marker in early stage gastric cancer. *Gastroenterology* 2010;139:213–225.e3.
41. Bockerstett KA, Lewis SA, Noto CN, Ford EL, Saenz JB, Jackson NM, Ahn TH, Mills JC, DiPaolo RJ. Single-cell transcriptional analyses identify lineage-specific epithelial responses to inflammation and metaplastic development in the gastric corpus. *Gastroenterology* 2020;159:2116–2129.e4.
42. Weis VG, Sousa JF, LaFleur BJ, Nam KT, Weis JA, Finke PE, Ameen NA, Fox JG, Goldenring JR. Heterogeneity in mouse spasmodic polypeptide-expressing metaplasia lineages identifies markers of metaplastic progression. *Gut* 2013;62:1270–1279.
43. Vange P, Bruland T, Munkvold B, Royset ES, Gleave M, Bakke I. Subtle protective roles of clusterin in gastric metaplasia after acute oxyntic atrophy. *Cell Mol Gastroenterol Hepatol* 2019;7:246–250.e1.
44. Takaishi S, Okumura T, Wang TC. Gastric cancer stem cells. *J Clin Oncol* 2008;26:2876–2882.
45. Hayakawa Y, Fox JG, Wang TC. The origins of gastric cancer from gastric stem cells: lessons from mouse models. *Cell Mol Gastroenterol Hepatol* 2017;3:331–338.
46. Bockerstett KA, DiPaolo RJ. Regulation of gastric carcinogenesis by inflammatory cytokines. *Cell Mol Gastroenterol Hepatol* 2017;4:47–53.
47. Fox JG, Wang TC. Inflammation, atrophy, and gastric cancer. *J Clin Invest* 2007;117:60–69.
48. Ollila S, Domenech-Moreno E, Laajanen K, Wong IP, Tripathi S, Pentimikko N, Gao Y, Yan Y, Niemela EH, Wang TC, Viollet B, Leone G, Katajisto P, Vaahtomeri K, Makela TP. Stromal Lkb1 deficiency leads to gastrointestinal tumorigenesis involving the IL-11-JAK/STAT3 pathway. *J Clin Invest* 2018;128:402–414.
49. Farshidpour M, Ahmed M, Junna S, Merchant JL. Myeloid-derived suppressor cells in gastrointestinal cancers: a systemic review. *World J Gastrointest Oncol* 2021;13:1–11.
50. Soutto M, Chen Z, Bhat AA, Wang L, Zhu S, Gomaa A, Bates A, Bhat NS, Peng D, Belkhiri A, Piazuelo MB, Washington MK, Steven XC, Peek R Jr, El-Rifai W. Activation of STAT3 signaling is mediated by TFF1 silencing in gastric neoplasia. *Nat Commun* 2019;10:3039.
51. Thiem S, Eissmann MF, Elzer J, Jonas A, Putoczki TL, Poh A, Nguyen P, Preaudet A, Flanagan D, Vincan E, Waring P, Buchert M, Jarnicki A, Ernst M. Stomach-specific activation of oncogenic KRAS and STAT3-dependent inflammation cooperatively promote gastric tumorigenesis in a preclinical model. *Cancer Res* 2016;76:2277–2287.
52. Willet SG, Lewis MA, Miao ZF, Liu D, Radyk MD, Cunningham RL, Burclaff J, Sibbel G, Lo HG, Blanc V, Davidson NO, Wang ZN, Mills JC. Regenerative proliferation of differentiated cells by mTORC1-dependent paligenesis. *EMBO J* 2018;37:e98311.
53. Koppens MAJ, Davis H, Valbuena GN, Mulholland EJ, Nasreddin N, Colombe M, Antanaviciute A, Biswas S, Friedrich M, Lee L, Oxford IBDCI, Wang LM, Koelzer VH, East JE, Simmons A, Winton DJ, Leedham SJ. Bone morphogenetic protein pathway antagonism by grem1 regulates epithelial cell fate in intestinal regeneration. *Gastroenterology* 2021;161:239–254.e9.
54. Worthley DL, Giraud AS, Wang TC. Stromal fibroblasts in digestive cancer. *Cancer Microenviron* 2010;3:117–125.
55. Lasota J, Dansonka-Mieszkowska A, Sobin LH, Miettinen M. A great majority of GISTs with PDGFRA mutations represent gastric tumors of low or no malignant potential. *Lab Invest* 2004;84:874–883.
56. Friis-Hansen L, Rieneck K, Nilsson HO, Wadstrom T, Rehfeld JF. Gastric inflammation, metaplasia, and tumor development in gastrin-deficient mice. *Gastroenterology* 2006;131:246–258.
57. Koh TJ, Goldenring JR, Ito S, Mashimo H, Kopin AS, Varro A, Dockray GJ, Wang TC. Gastrin deficiency results in altered gastric differentiation and decreased colonic proliferation in mice. *Gastroenterology* 1997;113:1015–1025.
58. Zavros Y, Eaton KA, Kang W, Rathinavelu S, Katukuri V, Kao JY, Samuelson LC, Merchant JL. Chronic gastritis in the hypochlorhydric gastrin-deficient mouse progresses to adenocarcinoma. *Oncogene* 2005;24:2354–2366.



59. Todisco A, Mao M, Keeley TM, Ye W, Samuelson LC, Eaton KA. Regulation of gastric epithelial cell homeostasis by gastrin and bone morphogenetic protein signaling. *Physiol Rep* 2015;3:e12501.
60. Wang TC, Dangler CA, Chen D, Goldenring JR, Koh T, Raychowdhury R, Coffey RJ, Ito S, Varro A, Dockray GJ, Fox JG. Synergistic interaction between hypergastrinemia and *Helicobacter* infection in a mouse model of gastric cancer. *Gastroenterology* 2000;118:36–47.
61. Dockray GJ. Topical review. Gastrin and gastric epithelial physiology. *J Physiol* 1999;518(Pt 2):315–324.
62. Merchant JL. Inflammation, atrophy, gastric cancer: connecting the molecular dots. *Gastroenterology* 2005;129:1079–1082.
63. Sigal M, Logan CY, Kapalczyńska M, Mollenkopf HJ, Berger H, Wiedenmann B, Nusse R, Amieva MR, Meyer TF. Stromal R-spondin orchestrates gastric epithelial stem cells and gland homeostasis. *Nature* 2017;548:451–455.
64. Correa P, Houghton J. Carcinogenesis of *Helicobacter pylori*. *Gastroenterology* 2007;133:659–672.
65. Choi E, Hendley AM, Bailey JM, Leach SD, Goldenring JR. Expression of activated Ras in gastric chief cells of mice leads to the full spectrum of metaplastic lineage transitions. *Gastroenterology* 2016;150:918–930.e13.
66. Mutoh H, Sakurai S, Satoh K, Tamada K, Kita H, Osawa H, Tomiyama T, Sato Y, Yamamoto H, Isoda N, Yoshida T, Ido K, Sugano K. Development of gastric carcinoma from intestinal metaplasia in *Cdx2*-transgenic mice. *Cancer Res* 2004;64:7740–7747.
67. Liu W, Yang LJ, Liu YL, Yuan DS, Zhao ZM, Wang Q, Yan Y, Pan HF. Dynamic characterization of intestinal metaplasia in the gastric corpus mucosa of *Atp4a*-deficient mice. *Biosci Rep* 2020;40:BSR20181881.
68. Ji T, Takabayashi H, Mao M, Han X, Xue X, Brazil JC, Eaton KA, Shah YM, Todisco A. Regulation and function of bone morphogenetic protein signaling in colonic injury and inflammation. *Am J Physiol Gastrointest Liver Physiol* 2017;312:G24–G33.
69. Li K, Wu H, Wang A, Charron J, Mishina Y, Habib SL, Liu H, Li B. mTOR signaling regulates gastric epithelial progenitor homeostasis and gastric tumorigenesis via MEK1-ERKs and BMP-Smad1 pathways. *Cell Rep* 2021;35:109069.
70. Blatter R, Tschupp B, Aretz S, Bernstein I, Colas C, Evans DG, Genuardi M, Hes FJ, Huneburg R, Jarvinen H, Laloo F, Moeslein G, Renkonen-Sinisalo L, Resta N, Spier I, Varvara D, Vasen H, Latchford AR, Heinimann K. Disease expression in juvenile polyposis syndrome: a retrospective survey on a cohort of 221 European patients and comparison with a literature-derived cohort of 473 SMAD4/BMPR1A pathogenic variant carriers. *Genet Med* 2020;22:1524–1532.
71. Vyas M, Yang X, Zhang X. Gastric hamartomatous polyps-review and update. *Clin Med Insights Gastroenterol* 2016;9:3–10.
72. Lieberman S, Beeri R, Walsh T, Schechter M, Keret D, Half E, Gulsuner S, Tomer A, Jacob H, Cohen S, Basel Salmon L, Mansur M, Berger R, Katz LH, Golomb E, Peretz T, Levy Z, Kedar I, King MC, Levy-Lahad E, Goldberg Y. Variable features of juvenile polyposis syndrome with gastric involvement among patients with a large genomic deletion of BMPR1A. *Clin Transl Gastroenterol* 2019;10:e00054.
73. Lee PJ, Zhang X, Shan P, Ma B, Lee CG, Homer RJ, Zhu Z, Rincon M, Mossman BT, Elias JA. ERK1/2 mitogen-activated protein kinase selectively mediates IL-13-induced lung inflammation and remodeling in vivo. *J Clin Invest* 2006;116:163–173.
74. Senger K, Pham VC, Varfolomeev E, Hackney JA, Corzo CA, Collier J, Lau VWC, Huang Z, Hamidzadeh K, Caplazi P, Peng I, Setiadi AF, Francis R, Paler-Martinez A, Kwon YC, Ramirez-Carrozzi V, Sun Y, Grigg PW, Roose-Girma M, Jeet S, Barck KH, Pham A, Ota N, Ha C, Stinson J, Guillory J, Tam L, Modrusan Z, Emson C, McKenzie BS, Townsend MJ, Carano RAD, Warming S, Vucic D, DeVoss J, Lee WP, Lill JR, Zarrin AA. The kinase TPL2 activates ERK and p38 signaling to promote neutrophilic inflammation. *Sci Signal* 2017;10:eaah4273.
75. Yokota S, Okabayashi T, Rehli M, Fujii N, Amano K. *Helicobacter pylori* lipopolysaccharides upregulate toll-like receptor 4 expression and proliferation of gastric epithelial cells via the MEK1/2-ERK1/2 mitogen-activated protein kinase pathway. *Infect Immun* 2010;78:468–476.
76. Daaka Y, Luttrell LM, Lefkowitz RJ. Switching of the coupling of the beta2-adrenergic receptor to different G proteins by protein kinase A. *Nature* 1997;390:88–91.
77. Zhang X, Zhang Y, He Z, Yin K, Li B, Zhang L, Xu Z. Chronic stress promotes gastric cancer progression and metastasis: an essential role for ADRB2. *Cell Death Dis* 2019;10:788.
78. Shi M, Yang Z, Hu M, Liu D, Hu Y, Qian L, Zhang W, Chen H, Guo L, Yu M, Song L, Ma Y, Guo N. Catecholamine-induced beta2-adrenergic receptor activation mediates desensitization of gastric cancer cells to trastuzumab by upregulating MUC4 expression. *J Immunol* 2013;190:5600–5608.
79. Di Giovanni V, Walker KA, Bushnell D, Schaefer C, Sims-Lucas S, Puri P, Bates CM. Fibroblast growth factor receptor-Frs2alpha signaling is critical for nephron progenitors. *Dev Biol* 2015;400:82–93.
80. Wang SS, Gu YF, Wolff N, Stefanus K, Christie A, Dey A, Hammer RE, Xie XJ, Rakheja D, Pedrosa I, Carroll T, McKay RM, Kapur P, Brugarolas J. Bap1 is essential for kidney function and cooperates with Vhl in renal tumorigenesis. *Proc Natl Acad Sci U S A* 2014;111:16538–16543.
81. Farmer DT, Mlcochova H, Zhou Y, Koelling N, Wang G, Ashley N, Bugacov H, Chen HJ, Parvez R, Tseng KC, Merrill AE, Maxson RE Jr, Wilkie AOM, Crump JG, Twigg SRF. The developing mouse coronal suture at single-cell resolution. *Nat Commun* 2021;12:4797.
82. Liu J, Krautberger AM, Sui SH, Hofmann OM, Chen Y, Baetscher M, Grgic I, Kumar S, Humphreys BD,

Hide WA, McMahon AP. Cell-specific translational profiling in acute kidney injury. *J Clin Invest* 2014; 124:1242–1254.

83. Poffenberger MC, Metcalfe-Roach A, Aguilar E, Chen J, Hsu BE, Wong AH, Johnson RM, Flynn B, Samborska B, Ma EH, Gravel SP, Tonelli L, Devorkin L, Kim P, Hall A, Izreig S, Loginicheva E, Beauchemin N, Siegel PM, Artyomov MN, Lum JJ, Zogopoulos G, Blagih J, Jones RG. LKB1 deficiency in T cells promotes the development of gastrointestinal polyposis. *Science* 2018;361:406–411.

H. Walker, PhD (Associate Professor, University of Pittsburgh) and Dr Juanita Merchant, MD, PhD (Professor, University of Arizona) for providing comments and editing the manuscript.

#### CRedit Authorship Contributions

Pawan Puri, DVM, PhD (Conceptualization: Lead; Data curation: Lead; Formal analysis: Lead; Funding acquisition: Lead; Investigation: Lead; Methodology: Lead; Project administration: Lead; Resources: Lead; Software: Lead; Supervision: Lead; Validation: Lead; Visualization: Lead; Writing – original draft: Lead; Writing – review & editing: Lead)

Garfield Grimmett (Conceptualization: Supporting; Data curation: Supporting; Formal analysis: Supporting; Investigation: Supporting; Methodology: Supporting; Writing – review & editing: Supporting)

Rawah Faraj, PhD (Data curation: Supporting; Formal analysis: Supporting; Methodology: Supporting; Writing – review & editing: Supporting)

Laurielle Gibson (Data curation: Supporting; Methodology: Supporting; Writing – review & editing: Supporting)

Ebony Gilbreath, DVM, PhD, DACVP (Data curation: Supporting; Formal analysis: Supporting; Investigation: Supporting; Methodology: Supporting; Validation: Supporting; Writing – review & editing: Supporting)

Bradley K. Yoder, PhD (Writing – review & editing: Supporting)

Received February 24, 2022. Accepted June 1, 2022.

#### Correspondence

Address correspondence to: Pawan Puri, DVM, PhD, Department of Biomedical Sciences, Tuskegee University College of Veterinary Medicine, A310 Patterson Hall, Tuskegee, AL 36088; e-mail: [ppuri@tuskegee.edu](mailto:ppuri@tuskegee.edu); tel: (334) 724-4486; fax: (334) 727-8177.

#### Acknowledgment

The authors thank Dr Temesgen Samuel (Professor, Tuskegee University College of Veterinary Medicine - TUCVM) for sharing research supplies and insightful discussions. The authors also thank RCMI Microscope Facility, Anatomic Pathology Facility, Comparative Medicine Resource Center staff at TUCVM. The authors also thank members of the Puri Lab for their technical assistance and comments. The authors give our sincere thanks to Dr William

#### Conflicts of interest

The authors disclose no conflicts.

#### Funding

The research in the principal investigator's (Pawan Puri) laboratory is supported by funding from the SC2GM130475 (Pawan Puri) grant awarded by the National Institute of General Medical Sciences. Other assistance: funds provided by the Tuskegee University College of Veterinary Medicine Health and Human Services grant HHS/HRSA #D34HP00001 and TU CBR/RCMI grant #U54MD007585. Laurielle Gibson was supported by National Institutes of Health/Summer Research Experience T35OD010432.

Supplementary Table 1. Antibodies

Antibody	Company	Catalog #	Application	Dilution
ARG1	Cell Signaling	93668	Immunofluorescence	1:500
ATP4A	Sigma	HPA039154	Western blotting Immunofluorescence	1:1000 1: 500
CD3	Cell Signaling	78588	Immunofluorescence	1:1000
CD44	Proteintech	15675-1-AP	Western blotting	1:1000
CHGA	Proteintech	23342-1-AP	Immunofluorescence	1:2000
ECAD	BD Bioscience	610181	Immunofluorescence	1:2000
P-CREB	Cell Signaling	9198	Western blotting Immunofluorescence	1:500 1:250
P-ERK	Cell Signaling	4370	Western blotting Immunofluorescence	1:1000 1:500
GIF	Sigma	HPA040774	Immunofluorescence	1:1000
GKN 1	Proteintech	19344-1-AP	Western blotting	1:500
GREM1	R & D	AF956-SP	Western blotting	1:1000
MIST1	Cell Signaling	14896	Immunofluorescence	1:1000
MUC2	Genetex	GTX100664	Immunofluorescence	1:500
MUC5B	Sigma	HPA008246	Western blotting Immunofluorescence	1:1000 1:1000
PCNA	Cell Signaling	13110	Western blotting Immunofluorescence	1:1000 1:500
PDGFRA	Cell Signaling	3174	Immunofluorescence	1:1000
PIGR	R & D	AF2800-SP	Western blotting	1:1000
RFP	Rockland	600-401-379	Immunofluorescence	1:1000
RFP	Rockland	200-101-379	Immunofluorescence	1:1000
P-STAT3	Cell Signaling	9145	Immunofluorescence	1:1000
P-SMAD1/5/9	Sigma	AB3848-I	Immunofluorescence	1:1000
P-SMAD1/5	Cell Signaling	9516	Western blotting	1:1000
SMAD5	Cell Signaling	12534	Western blotting	1:1000
SMA	Sigma	A5228	Immunofluorescence	1:2000
VIL1	Proteintech	16488-1-AP	Immunofluorescence	1:1000
VIM	Cell Signaling	5741	Immunofluorescence	1:1000
Biotin Griffonia (Bandeiraea) Simplicifolia Lectin II (GSII)	Vector Lab	BK-3000	Immunofluorescence	1:1000
Fluorescein labeled Dolichos Biflorus Agglutinin (DBA)	Vector Labs	FL-1031	Immunofluorescence	1:500
Ulex Europaeus Agglutinin I (UEA I), Rhodamine	Vector Labs	RL-1062-2	Immunofluorescence	1:1000
DyLight*488 STREPTAVIDIN	Vector Labs	SA-5488-1	Immunofluorescence	1:1000
Anti-rabbit IgG HRP-linked antibody	Cell Signaling	7074	Immunofluorescence	1:1000
Anti-rabbit IgG HRP-linked antibody	Cell Signaling	7076	Immunofluorescence	1:1000
Alexa Fluor® 488-conjugated AffiniPure donkey anti-mouse IgG (H+L)	Jackson ImmunoResearch	715-545-150	Immunofluorescence	1:1000
Donkey anti-rabbit IgG (H+L) highly cross-adsorbed secondary antibody, Alexa Fluor 488	Thermo Fisher Scientific	A-21206	Immunofluorescence	1:1000
Donkey anti-rat IgG (H+L) highly cross- adsorbed secondary antibody, AlexaFluor 488	Thermo Fisher Scientific	A21208	Immunofluorescence	1:1000
Alexa Fluor® 594-conjugated AffiniPure donkey anti-goat†† IgG (H+L)	Jackson ImmunoResearch	705-585-003	Immunofluorescence	1:1000
Donkey anti-rabbit IgG (H+L) highly cross-adsorbed secondary antibody, AlexaFluor 594	Thermo Fisher Scientific	A21207	Immunofluorescence	1:1000
Donkey anti-mouse IgG (H+L) highly cross-adsorbed secondary antibody, AlexaFluor 594	Thermo Fisher Scientific	A21203	Immunofluorescence	1:1000